# Thermodynamics of *d*-wave superconductors in a magnetic field

I. Vekhter,[1,*] P. J. Hirschfeld,[2] and E. J. Nicol[3]
[1]*Theoretical Division, Los Alamos National Laboratory, Los Alamos, New Mexico 87545*
[2]*Department of Physics, University of Florida, Gainesville, Florida 32611*
[3]*Department of Physics, University of Guelph, Guelph, Ontario, Canada N1G 2W1*
(Received 2 November 2000; published 23 July 2001)

We investigate the thermodynamic properties of a two-dimensional *d*-wave superconductor in the vortex state using a semiclassical approach, and argue that such an approach is valid for the analysis of the experimental data on high-temperature superconductors. We develop a formalism where the spatial average of a physical quantity is written as an integral over the probability density of the Doppler shift, and evaluate this probability density for several model cases. The approach is then used to analyze the behavior of the specific heat and the nuclear magnetic resonance (NMR) spin-lattice relaxation rate in a magnetic field. We compare our results with the experimental measurements, and explain the origin of the discrepancy between the results from different groups. We also address the observability of the recently predicted fourfold oscillations of the specific heat for the magnetic field parallel to the copper oxide planes. We consider both the orbital and the Zeeman effects, and conclude that at experimentally relevant temperatures Zeeman splitting does not appreciably reduce the anisotropy, although it does change the field dependence of the anisotropic specific heat. We predict a scaling law for the nonexponentially decaying NMR magnetization, and discuss different approaches to the effective relaxation rate.

DOI: 10.1103/PhysRevB.64.064513 PACS number(s): 74.72.−h, 74.25.Bt

## I. INTRODUCTION

Despite significant recent advances we still lack a complete understanding of the physics of low-energy excitations in the vortex state of unconventional superconductors. High-temperature superconductors (HTSC's) are an example of a system where theoretical predictions can be checked against a large body of experimental evidence. In zero field these materials have a *d*-wave superconducting energy gap, with nodes along the diagonals of the Brillouin zone, and consequently a finite density of low-energy excitations.[1] Moreover, it is believed that at temperatures low compared to the transition temperature, $T \ll T_c$, these excitations are reasonably well described by the Landau quasiparticles, even though such an approach fails in these materials at higher energies. A variety of experimentally measured quantities such as the electronic specific heat,[2–6] effective penetration depth from muon spin rotation,[7] spin-lattice relaxation rate,[8,9] and thermal conductivity[10–12] are available to test the predictions of theories.

In this work we discuss the influence of the magnetic field on the thermodynamic quantities in the vortex state of the unconventional superconductor, and, in particular, address the question of how these properties depend on the structure of the vortex state. We concentrate on the behavior of the density of states and the electronic specific heat and the spin-lattice relaxation of the nuclear magnetic resonance (NMR) magnetization. There exist several theoretical approaches to the analysis of the thermodynamic quantities in the vortex state of unconventional superconductors. We employ here a semiclassical approach,[13,14] which has been successful in describing the field dependence of a variety of the physical quantities.[13–15] It is an approximate description, and in the next section we discuss the region of its validity and the grounds for our belief that it is applicable to the present problem. Section III introduces the basic model of the nodal quasiparticles and the idea that the physical quantities in the vortex state can be obtained by calculating the spatial average of their local values, computed with the help of the semiclassical approach.

Until now such spatial averages have only been done analytically in an oversimplified model of a single vortex.[13–18] In this paper we introduce a generalization of these approaches by rewriting the spatial average as an average over the probability density of the Doppler shift of the quasiparticle energy in the presence of the superflow. Restating the problem in this language enables us to introduce several model distributions of the probability density, discussed in Sec. IV, and investigate how the physical quantities obtained within the semiclassical framework depend on these distributions and on the structure of the vortex state. We obtain the energy and field dependence of the density of states for the geometries with the magnetic field applied both normal to the superconducting planes and in the plane in Sec. V. This density of states is used to analyze the behavior of the electronic specific heat in HTSC's. We obtain the energy scales relevant to the high-temperature superconductors in the vortex state, and suggest a resolution to the origin of the disagreement between different experimental groups regarding the magnitude of the field-dependent term in the specific heat and the form of the scaling function; this is the content of Sec. VI. In the same section we address the question of the observability of the oscillations in the specific heat for the magnetic field applied in the superconducting plane as a function of the angle between the field and the nodal directions. These oscillations have been recently predicted,[17,19] but so far have not been observed. Part of the difficulty may stem from the smallness of the in-plane Doppler energy scale, as inferred from the experimental measurements; it has recently been argued that the Zeeman splitting reduces the observed oscillations significantly,[20] and we investigate its effect in detail in this work.

 

Section VII is devoted to the effect of the nonuniform density of states on the spin-lattice relaxation time. This nonuniformity leads to a nonexponential decay of the magnetization and to a field dependence of the effective relaxation rate;[16] here we show that the effective relaxation rate depends on the structure of the vortex state, and obtain an approximate form for it. We also predict a scaling law for the magnetization decay that can be checked directly. The effect of impurities on the density of states is briefly addressed in Sec. VIII. We expect these effects to be very important for the discussion of the transport properties that we defer to a later publication. Finally we summarize our findings and discuss some open questions.

## II. SEMICLASSICAL APPROXIMATION

HTSC's are extreme type II superconductors (the ratio of the London penetration depth $\lambda_L$ to the coherence length $\xi_0$ is large, $\lambda_L/\xi_0 \sim 100$), and are in the mixed state over the range of applied fields $H$, from a few hundred gauss to well in excess of 50 T in $YBa_2Cu_3O_{7-\delta}$ (YBCO) and $Bi_2Sr_2CaCu_2O_{8+\delta}$ (Bi-2212 or BSCCO) near optimal doping. In the mixed state the magnetic field penetrates the bulk of the superconductor in the form of vortices, which consist of the cores, where the superconducting order parameter is suppressed, and circulating supercurrents around them. The vortex core size is of the order of the coherence length, $\xi_0 \sim 15$ Å ,[21,22] while the average intervortex distance can be estimated by imposing the requirement of one flux quantum $\Phi_0 = hc/2e$ per vortex, or $d/2 = R = \sqrt{\Phi_0/\pi B}$, where $B$ is the internal field. At typical experimentally accessible fields (1–20 T) $\lambda_L \gg d \gg \xi_0$, the magnetization due to the vortex lattice is small, and the internal field can be replaced by the applied field $H$ so that $d\sqrt{H} \sim 500$ Å $T^{1/2}$. The actual distance differs from the average value $d$ by a numerical factor of the order of unity, which depends on the structure of the vortex state; the vortices in HTSC's may form a regular lattice (as they do in YBCO and in Bi-2212 at low fields[23,24]) or be moderately disordered (as in Bi-2212 at higher fields[22]).

In the experimentally relevant fields, $H_{c1} \ll H \ll H_{c2}$, where $H_{c1}$ ($H_{c2}$) is the lower (upper) critical field, there may exist two types of low-energy excitations. First, as in conventional, *s*-wave materials with an isotropic gap, there may be a branch of low-energy fermionic excitations bound to the vortex cores.[25] Theoretical studies of the Bogoliubov-deGennes equations, however, suggest that there are no truly bound states in the vortex cores of a *d*-wave superconductor.[26,27] Experimental evidence also indicates that there is at most one such state in the vortex cores of YBCO and Bi-2212.[23,22] Therefore the properties of the mixed state of *d*-wave superconductors are dominated by the ''extended'' quasiparticle states in the bulk. These states are formed when quasiparticles with momenta close to the position of the nodes of the gap, $\Delta_{\mathbf{k}}$, in the momentum space (and therefore with a small gap) interact with the supercurrents in the vortex state. Most of the theoretical work has explored the properties of these states.

Very significant progress has been made by utilizing the semiclassical approach, which treats the momentum and the position of the quasiparticle as commuting variables. It is valid when the wave function of a quasiparticle can be replaced by its envelope on the length scales exceeding the coherence length, i.e., when $k_f \xi_0 \gg 1$, where $k_f$ is the inverse Fermi wavelength. In that method the effect of the supercurrents is accounted for by introducing a Doppler shift into the quasiparticle energy spectrum,[28,29,13,14] $E'(\mathbf{k},\mathbf{r}) = E(\mathbf{k}) + \epsilon(\mathbf{k},\mathbf{r})$. Here $E(\mathbf{k})$ is the energy of a quasiparticle with momentum $\mathbf{k}$ in the absence of the field measured with respect to the chemical potential. In a two-dimensional *d*-wave superconductor this spectrum is conical (massless anisotropic Dirac spectrum): $E(\mathbf{k}) \approx \pm\sqrt{v_f^2 k_\perp^2 + v_\Delta^2 k_\parallel^2}$, where the Fermi velocity $v_f$ is associated with the dispersion of the quasiparticles in the direction normal to the Fermi surface (component $k_\perp$ of the momentum), while $v_\Delta \sim \Delta_0/k_f$ is the slope of the gap at the node associated with the dispersion of the quasiparticles along the Fermi surface ($k_\parallel$). The Doppler shift, $\epsilon(\mathbf{k},\mathbf{r}) = \mathbf{v}_s \cdot \mathbf{k}$ depends on the quasiparticle momentum and the local value of the supervelocity, $\mathbf{v}_s(\mathbf{r})$. This shift in the energy is an exact result for a uniform supercurrent,[30] where it reflects the pairing of the electrons with a finite center-of-mass momentum. In the simplest picture such an approach remains valid for a nonuniform current for as long as the spatial variations of $\mathbf{v}_s$ are slow on the scale of the spatial extent of the Cooper pair, $\xi_0$. In superconductors with nodes in the energy gap, the Doppler shift may exceed the local (in the momentum space) gap, and leads to an increase in the density of the unpaired quasiparticles: even at $T=0$ for some positive energies $E$ the shifted energy $E'$ is negative so that the corresponding states become occupied. In the context of *d*-wave superconductors this was emphasized by Yip and Sauls,[29] who investigated the effect of the screening currents in the Meissner state on the superfluid density. These currents vary on the scale of the penetration depth $\lambda_L \gg \xi_0$, so that the Doppler shift description is appropriate, and result in a linear dependence of the effective penetration depth on the applied field for certain experimental geometries.[29] However, so far the predicted dependence has not been confirmed experimentally.[31]

Similar physics is at play in the dilute vortex limit. At distances small compared to the penetration depth, supercurrents around an isolated vortex are inversely proportional to the distance from the center of the vortex, $r$; for $\xi_0 \ll r \ll \lambda_L$ the supervelocity field is $|\mathbf{v}_s| = \hbar/2mr$, where $m$ is the quasiparticle mass. Consequently, the requirement of the slowness of the variation of $\mathbf{v}_s$, which can be written as $|\nabla \mathbf{v}_s| \xi_0 \ll \mathbf{v}_s$ (two particles comprising the Cooper pair ''see'' the same velocity), is satisfied at $r \gg \xi_0$, justifying the use of the semiclassical approach outside of the core and therefore for the analysis of the extended quasiparticle excitations at energies low compared to the gap maximum. Such an analysis for a single vortex in *d*-wave superconductors was first carried out in a landmark paper by Volovik,[13] who showed that the density of the extended quasiparticles at low temperature $T$ varies as $\sqrt{H}$. This result was confirmed first by Moler *et al.*[2] and subsequently by other groups[3–5] from the measurements of the electronic specific heat in an applied magnetic field. Numerical studies of the tight-binding model are also in

qualitative agreement with this result.[32] Moreover Volovik has shown that the density of the extended quasiparticles dominates that of the states bound to the vortex core even if the latter set is treated semiclassically, as a quasicontinuum[13] (as it would be in a superconductor with a long coherence length). Together with the numerical studies of Refs. 26 and 27 this result provided further theoretical support for neglecting the core states in the analysis of the properties of the vortex state in unconventional superconductors.

The semiclassical approach was incorporated into the Green's function formalism by Kübert and Hirschfeld,[14] and used in that form to analyze thermodynamic and transport properties of the high-$T_c$ cuprates in the vortex state.[15–17] In particular, accounting for the impurity scattering in this framework has significantly improved the agreement between the theory and the measurements of the electronic specific heat,[14] and the field dependence of the low-temperature thermal conductivity[10] is in qualitative agreement with the results of a semiclassical calculation.[15] In the semiclassical approach the effect of the magnetic field is contained in the new energy scale associated with the Doppler shift, $E_H = v_f/d$, and the behavior of the physical properties is determined by the competition between this energy, the temperature, and the impurity scattering rate. Photoemission measurements on high-$T_c$ compounds suggest[33,34] that $v_f \simeq (1.5 - 2.5) \times 10^7$ cm/s leading to $E_H \sim 30\sqrt{H}$ K T$^{-1/2}$.

For a long time, understanding of the low-energy excitations in the vortex state beyond this semiclassical picture has proved elusive. The difficulties stem in part from the need to treat on equal footing the applied magnetic field and the superconducting currents (semiclassical approach treats the supercurrents classically). Attempts have been made to take as a starting point the Landau quantization of the quasiparticle states, and include the effects of supercurrents perturbatively;[35,36] however, since the supervelocity field is long ranged and singular at the position of each vortex, the Landau levels are strongly mixed, making a detailed analysis difficult.[37]

The most significant progress has been made in a recent work by Franz and Tešanović,[38] who have introduced a gauge transformation that takes into account both the supercurrent distribution and the magnetic field. In their approach the problem is mapped onto that of nodal Dirac fermions in an effective zero average magnetic field interacting with effective scalar and vector potentials that are periodic in the unit cell of the vortex lattice. Both Franz and Tesanovic[38] and Marinelli *et al.*[39] have studied the band structure of the nodal quasiparticles for perfectly periodic vortex lattices for various values of the anisotropy of the Dirac spectrum, $\alpha_D = v_f/v_\Delta$.

There are two reasons for expecting modifications to the semiclassical spectrum. The first is related to the singular spatial structure of the supervelocity field. One flux quantum associated with a single vortex means that the superconducting order parameter, or, equivalently, the wave function of a Cooper pair (charge $2e$) is single valued and has a phase winding of $2\pi$ around each vortex. As emphasized in Ref. 38, the semiclassical approach transfers this phase winding equally to each of the quasiparticles forming the Cooper pair (each having charge $e$). Consequently, their wave functions change phase by $\pi$ around a vortex line (Aharonov-Bohm phase), leading to the necessity of introducing branch cuts and to the problem of multivalued wave functions in the full quantum mechanical treatment. However, the semiclassical approximation is only valid for large quantum numbers, that is for the quasiparticles for which the total phase of the wave function, accumulated as the electron moves around the vortex, is large. The wave function of an electron circling a vortex at a distance $r$ from the vortex center acquires a phase $2\pi k_f r$, compared to an extra Aharonov-Bohm phase $\pi$ from the supervelocity field. For the analysis of the extended states ($r \gg \xi_0$) in the semiclassical approach (valid at $k_f \xi_0 \gg 1$), $k_f r \gg 1$, so that if the phase of the wave function is changed by $\pi$, it still corresponds to the quasiclassical state with essentially the same energy and momentum. Since $\xi_0 \sim v_f/\Delta_0$, we can rewrite the condition for the applicability of the semiclassical method, $k_f \xi_0 \gg 1$, as $\alpha_D = v_f/v_\Delta \gg 1$. Indeed, the work of Refs. 38,39 has shown that for large anisotropy of the Dirac cone the semiclassical approach remains valid down to the lowest energies. Since $\alpha \simeq 14$ for YBCO (Ref. 10), and $\alpha \simeq 20$ for Bi-2212 (Refs. 40 and 34) this is the parameter range relevant for the study of HTSC's. In a very recent preprint Mel'nikov has shown that the Aharonov-Bohm phase leads to a different result for the quasiparticle density at distances $r \gg \lambda_L$, while in the range $\xi_0 \ll r \ll \lambda_L$ the semiclassical results hold.[41] Once again, since in the field range where most experimental measurements are done the intervortex distance $d \ll \lambda_L$ this result suggests that the semiclassical approach is adequate for the analysis of these experiments.

Quantum mechanical treatment is nevertheless needed for accurate description of the states at very low energies. Kopnin and Volovik[42] have considered the effect of the magnetic field on the nodal quasiparticles perturbatively, and found that the spacing between quantum mechanical levels of the near-nodal quasiparticles, for which the spatial extent of the wave function is comparable to the intervortex distance, is $E_{KV} = v_\Delta/d = E_H/\alpha_D$. Therefore they have argued that below this energy scale the semiclassical approach becomes invalid. For $\alpha \sim 15$ this energy scale is of the order of a few kelvin per square root of tesla. However, the specific-heat measurements show no crossover to a novel behavior at that scale,[5] and the measurements of the thermal conductivity below 0.5 K in fields of up to 8 T are in agreement with the semiclassical calculations.[10]

This crossover was recently investigated by Marinelli *et al.*[39] and Knapp *et al.*[43] by comparing numerically the quantum mechanical and semiclassical results for the density of states. The picture that emerges from their analysis is that small differences between the two approaches begin to appear below the Kopnin-Volovik crossover scale. These are rather minor, and the qualitative difference between the two results does not appear down to a much smaller crossover scale, exponentially small in $\alpha_D$.[43,44] Since in real samples the presence of impurity scattering and the disorder in the vortex lattice always smear out the energy structure on small scales, we therefore expect that for the purposes of comparison with the measurements of the thermodynamic quantities,

the semiclassical description is adequate.

Therefore for the parameter range relevant to the study of most real unconventional superconductors, the semiclassical approach reproduces the energy spectrum of the near-nodal quasiparticles in the vortex state to a high degree of accuracy. Moreover, presently it remains the only approach that is capable of including the effect of impurity scattering into the analysis, and we use it hereafter.

## III. SEMICLASSICAL APPROACH TO THE VORTEX STATE

### A. Nodal approximation

The semiclassical approximation takes as its starting point a Fermi-liquid description of the nodal quasiparticles, so that in the absence of a magnetic field the Green's function in the particle-hole (Nambu) space is given by the Bardeen-Cooper-Schrieffer form with an anisotropic gap,

$$G(\mathbf{k},\omega_n)=-\frac{i\omega_n\hat{\tau}_0+\Delta_{\mathbf{k}}\hat{\tau}_1+\zeta_{\mathbf{k}}\hat{\tau}_3}{\omega_n^2+\zeta_{\mathbf{k}}^2+\Delta_{\mathbf{k}}^2}. \tag{1}$$

Here $\hat{\tau}_i$ for $i=0\cdots3$ are the Pauli matrices ($\hat{\tau}_0$ is the unit matrix), $\omega_n=\pi T(2n+1)$ is the Matsubara frequency, and $\zeta_{\mathbf{k}}$ is the energy of a quasiparticle with momentum $\mathbf{k}$ measured relative to the chemical potential. We consider a two-dimensional Fermi surface with an energy gap of $d_{x^2-y^2}$ symmetry given by $\Delta_{\mathbf{k}}=\Delta_0(k_x^2-k_y^2)/k^2$. Low-energy properties depend only on the nodal quasiparticles, and are only functions of the parameters entering the linearized dispersion near nodes at position $\mathbf{k}_n$. As $\zeta_{\mathbf{k}}\approx\mathbf{v}_f\cdot(\mathbf{k}-\mathbf{k}_n)$, and $\Delta_{\mathbf{k}}\approx\mathbf{v}_\Delta\cdot(\mathbf{k}-\mathbf{k}_n)$ near a node, the poles of the Green's function after analytic continuation to the real axis, $i\omega_n\to\omega+i\delta$, are located at energies

$$E(\mathbf{k})=\pm\sqrt{\zeta_{\mathbf{k}}^2+\Delta_{\mathbf{k}}^2}\approx\pm\sqrt{v_f^2k_\perp^2+v_\Delta^2k_\parallel^2}, \tag{2}$$

where $k_\perp$ and $k_\parallel$ are the components of $\mathbf{k}-\mathbf{k}_n$ normal to and along the Fermi surface respectively. We parametrize the Fermi surface near each of the four nodes not by the momenta $k_\perp$ and $k_\parallel$, but by the quasiparticle energy $E$ and the angle $\Theta$ defined as

$$v_fk_\perp=E\sin\Theta, \tag{3}$$

$$v_\Delta k_\parallel=E\cos\Theta. \tag{4}$$

The energy cutoff is chosen to preserve the volume of the Brillouin zone of the crystal lattice, so that for a square lattice with the periodicity $a$, it is set at $E_0=\sqrt{\pi v_fv_\Delta}/a$.[45] By making this choice we extend the conical dispersion law beyond the maximal gap value, $\Delta_0$. This leads to logarithmic, in $E_0/\Delta_0$, corrections to the quantities that depend on the cutoff energy. Since $v_\Delta\sim\Delta_0/k_f$ and $k_f\sim\pi/a$, we obtain $E_0\sim\sqrt{E_f\Delta_0}$, where $E_f$ is the Fermi energy. In the high-$T_c$ materials $E_f\sim3-10\Delta_0$, and, consequently, the choice of $E_0$ as the cutoff energy does not affect the results significantly. Therefore near each node the Green's function at real frequencies can be written as

$$\hat{G}(E,\theta;\omega)=\frac{\tilde{\omega}\hat{\tau}_0+E\cos\Theta\,\hat{\tau}_1+E\sin\Theta\,\hat{\tau}_3}{\tilde{\omega}^2-E^2}. \tag{5}$$

In writing Eq. (5) we have replaced the bare frequency $\omega$ by the renormalized frequency $\tilde{\omega}$ to include the effect of impurity scattering. We account for isotropic strong (phase shift $\pi/2$) impurity scattering in the framework of a self-consistent $T$-matrix approximation, and consider a particle-hole symmetric system, so that the only nonvanishing component of the self-energy is proportional to $\hat{\tau}_0$.[46] Therefore the effect of impurities is to replace in the Green's function $\omega$ by its renormalized value, $\tilde{\omega}=\omega-\Sigma(\tilde{\omega})$, with the self-consistency condition

$$\Sigma(\tilde{\omega})=-n_i\left[\sum_{\mathbf{k}}G_{11}(\tilde{\omega})\right]^{-1}, \tag{6}$$

where $n_i$ is the impurity concentration. In the nodal approximation the integral over the Brillouin zone can be written as a sum over the nodal regions

$$\sum_{\mathbf{k}}G_{11}=\sum_{nodes}\frac{1}{v_fv_\Delta}\int_0^{E_0}\frac{EdE}{2\pi}\int_0^{2\pi}\frac{d\Theta}{2\pi}\frac{\tilde{\omega}}{\tilde{\omega}^2-E^2}. \tag{7}$$

Writing $\tilde{\omega}=\omega_1+i\omega_2$, we obtain for $E_0\gg|\tilde{\omega}|$

$$\sum_{\mathbf{k}}G_{11}=-\frac{2}{\pi}\frac{\omega_1+i\omega_2}{v_fv_\Delta}\left[\ln\frac{E_0}{\sqrt{\omega_1^2+\omega_2^2}}+i\arctan\frac{\omega_1}{\omega_2}\right]. \tag{8}$$

The well-known relationships for the density of states in the pure limit ($\omega_2=0,\omega_1=\omega$), and for the residual density of states in the presence of impurities ($\omega_1=0,\omega_2=\gamma$) follow easily (cf. Ref. 45) from

$$N(\omega)=-\frac{1}{\pi}\sum_{\mathbf{k}}\mathrm{Im}\ G_{11}(\mathbf{k},\omega), \tag{9}$$

to give

$$N(\omega)=\frac{|\omega|}{\pi v_fv_\Delta},\quad \text{pure limit} \tag{10}$$

$$N(0)=\frac{2}{\pi^2}\frac{\gamma}{v_fv_\Delta}\ln\frac{E_0}{\gamma},\quad \text{unitarity.} \tag{11}$$

The self-consistency condition $\omega_1+i\omega_2=\omega-\Sigma(\tilde{\omega})$ for the latter case is (cf. Ref. 47)

$$\gamma^2=\frac{\pi}{2}n_iv_fv_\Delta\left[\ln\frac{E_0}{\gamma}\right]^{-1}. \tag{12}$$

### B. Doppler shift

In the semiclassical approach to the vortex state the presence of a superflow is accounted for by introducing the Doppler shift into the energy $\omega\to\omega+\boldsymbol{\epsilon}(\mathbf{k},\mathbf{r})$,[13,14] where

$$\epsilon(\mathbf{k},\mathbf{r}) = \mathbf{v}_s(\mathbf{r}) \cdot \mathbf{k}, \tag{13}$$

and $\mathbf{v}_s(\mathbf{r})$ is the supervelocity field at a position $\mathbf{r}$ due to all vortices. It was demonstrated by Kübert and Hirschfeld[14] that to very high accuracy the Doppler shift at the node $\mathbf{k}_n$ can be used to approximate the Doppler shift for the entire nodal region. Therefore the Green's function near each node can be written as

$$\hat{g}(E,\Theta;\omega;\mathbf{r}) = \hat{G}(E,\Theta;\omega+\epsilon_n(\mathbf{r})), \tag{14}$$

where $\hat{G}$ is given by Eq. (5), $n$ labels the nodes, and $\epsilon_n(\mathbf{r}) = \mathbf{v}_s(\mathbf{r}) \cdot \mathbf{k}_n$. For a *d*-wave superconductor there are two pairs of nodes such that $\mathbf{k}_1 = -\mathbf{k}_3$ and $\mathbf{k}_2 = -\mathbf{k}_4$, so that the possible values for the Doppler shift are $\pm\epsilon_1$ and $\pm\epsilon_2$.

In principle now all the physical quantities can be computed with the help of this Green's function. Several comments have to be made about the assumptions implicitly present in such calculations. First, we neglect all inelastic processes. Second, there is no additional quasiparticle damping due to the presence of the vortices: in the absence of impurities the lifetime of a quasiparticle defined by the pole of the Green's function in Eq. (14) is infinite. The scattering of the nodal quasiparticles by vortices depends strongly on the nature of the vortex cores; in the high-$T_c$ materials this is an unresolved problem.[48,49] If the point of view is taken that the core is identical to that of a BCS-like superconductor, the neglect of vortex scattering is reasonable for a vortex lattice with long-range order, and it remains valid when only short-range order exists provided that the lifetime is restricted by the impurity scattering rather than vortex disorder. The role of disorder in the vortex lattice is especially important for transport properties, where there is a competition between the increase in the density of quasiparticles and the change in the transport lifetime in an applied field; several authors have analyzed its consequences,[15,51,52] and some questions remain unresolved.[50,52,53] Scanning-tunneling spectroscopy measurements suggest that the vortex lattice is ordered in YBCO,[23] and that short-range order is present in Bi-2212,[22] therefore in that case the assumption is justified. We note that thermodynamic quantities, such as the density of states, depend on a single energy scale, $E_H = v_f/d$ even in a disordered vortex state in the absence of strong pinning, and this dependence appears to be nearly identical for the ordered and disordered vortex lattices.[50] Therefore we expect that the results obtained within the semiclassical approach remain at least qualitatively valid even for a strongly disordered lattice.

Third, in the analysis of the impurity scattering this approach assumes that the positions of vortices and of impurities are uncorrelated. The self-energy given by Eq. (6) is obtained after averaging over the positions of impurities, and solving this equation with the Doppler shift included in the Green's function implies that the impurity average and the spatial average are taken independently.

Finally, in the discussion so far we have neglected the Zeeman splitting altogether; this is justified when the Doppler energy scale exceeds the Zeeman shift. In the absence of spin-orbit coupling the Zeeman shift is $\mu H \approx 0.67H$ K T$^{-1}$, while the Doppler shift is $E_H \simeq 30\sqrt{H}$ K T$^{-1/2}$; consequently the two become comparable only at $H_{cross} \sim 10^3$ T, and hence the Zeeman splitting is irrelevant. On the other hand, for the field applied in the plane, the coefficient in the Doppler shift is much reduced,[17] and the Zeeman splitting is relevant for some experimental geometries.[20] Consequently, we will revisit this question in the analysis for this configuration.

If we know how to express a physical quantity $F$ in terms of the Green's function we can now compute its local value $F(\mathbf{r})$ with the local Green's function given by Eq. (14). We then approximate the field-dependent measured value $F(H)$ by the spatial average of $F(\mathbf{r})$[14,15]

$$F(H) = \frac{1}{A}\int d^2\mathbf{r} F(\epsilon_1(\mathbf{r}), \epsilon_2(\mathbf{r})), \tag{15}$$

where the integral is taken over the part of a unit cell of the vortex lattice (with the area $A$) in real space where the Doppler shift is much smaller than the gap maximum. Therefore the integration is to be cut off at distances of the order of $\xi_0$ from the center of each vortex. In practice in many cases the contribution of the core region ($r \leqslant \xi_0$) is small due to the geometric effect (integrals are weighted with the surface area $rdr$) and the integral can be extended to the entire unit cell. We note that the averaging procedure is often nontrivial for response functions; for the thermal conductivity $\kappa$, for example, $\kappa(\mathbf{r})$ or $1/\kappa(\mathbf{r})$ are averaged depending on the relative orientation of the magnetic field and the heat current.[15,51] The average in Eq. (15) depends on the distribution of vortices. In practice, this spatial average has been computed analytically only for the supervelocity field corresponding to an isolated flux line, cut off at the average intervortex distance,[13–17] and numerically for the pancake liquid state.[52]

The starting point of our approach, which simplifies calculations and makes possible a generalization of the semiclassical method to an arbitrary configuration of vortices is to rewrite the average as the integral over the *probability distribution* of the Doppler shift for a particular vortex configuration. There are, in general, two types of local quantities, and therefore of averaging procedures, which are required. The density of states in the absence of impurity scattering, for example, is a direct sum of the contributions from each node,

$$\begin{aligned} N(\omega,\mathbf{r}) &= -\frac{1}{2\pi}\mathrm{Im}\left\{\sum_{\mathbf{k}} \mathrm{Tr}\,\hat{G}(\mathbf{k},\omega)\right\} \\ &\approx -\frac{1}{2\pi}\mathrm{Im}\left\{\sum_{\substack{\alpha=\pm \\ n=1,2}} \int \frac{dE d\Theta}{4\pi^2 v_f v_\Delta} \right. \\ &\left. \times \mathrm{Tr}\,\hat{G}(E,\Theta;\omega+\alpha\epsilon_n(\mathbf{r}))\right\}, \end{aligned} \tag{16}$$

and can consequently be expressed as an integral over the probability density of the Doppler shift *at a single node*,

$$N(\omega,H) = \frac{1}{2}\sum_{\alpha=\pm}\int_{-\infty}^{+\infty} d\epsilon N(\omega+\alpha\epsilon)\mathcal{P}(\epsilon), \tag{17}$$

where

$$\mathcal{P}(\epsilon)=\frac{1}{A}\int d^2\mathbf{r}\,\delta(\epsilon-\mathbf{v}_s(\mathbf{r})\cdot\mathbf{k}_n). \tag{18}$$

Such an approach has been recently used to analyze the behavior of the interlayer conductivity in the vortex liquid state,[52] where the function $\mathcal{P}$ was determined from numerical simulations. A similar method (although with an unrealistic distribution, see below) has been used in the analysis of the thermal conductivity.[54,50]

However, in general the function $F$ depends on the values for the Doppler shift at two inequivalent nodes, $\epsilon_1$ and $\epsilon_2$, and the corresponding average can be written as

$$F(H)=\int_{-\infty}^{+\infty} d\epsilon_1 d\epsilon_2 F(\epsilon_1,\epsilon_2)\mathcal{L}(\epsilon_1,\epsilon_2), \tag{19}$$

$$\mathcal{L}(\epsilon_1,\epsilon_2)=\frac{1}{A}\int d^2\mathbf{r}\,\delta(\epsilon_1-\mathbf{v}_s(\mathbf{r})\cdot\mathbf{k}_1)\,\delta(\epsilon_2-\mathbf{v}_s(\mathbf{r})\cdot\mathbf{k}_2), \tag{20}$$

where $\mathbf{k}_1$ and $\mathbf{k}_2$ label two nearest nodes. This is the case, for example, for the density of states in the presence of impurity scattering, since the self-energy [implicitly present in the Green's function in Eq. (16)] contains the sum over the nodes, see Eq. (6), and therefore depends on both $\epsilon_1$ and $\epsilon_2$. In general, the function $\mathcal{L}$ has to be even in both $\epsilon_1$ and $\epsilon_2$, and symmetric under the interchange $\epsilon_1\leftrightarrow\epsilon_2$; in all the cases considered below it depends on a single variable $\epsilon_1^2+\epsilon_2^2$.

Now all the relevant information about the structure of the vortex state is contained in the functions

$$\mathcal{L}(\epsilon_1,\epsilon_2)=\mathcal{L}'(\epsilon_1^2+\epsilon_2^2)$$

and

$$\mathcal{P}(\epsilon)=\int d\epsilon_1\mathcal{L}(\epsilon,\epsilon_1), \tag{21}$$

and therefore to analyze the field dependence of the physical quantities we first focus on determining these probability densities.

## IV. PROBABILITY DENSITY FOR THE DOPPLER SHIFT

The distributions $\mathcal{P}$ and $\mathcal{L}$ can be determined numerically for an arbitrary configuration of vortices. Here we are interested in making progress analytically, and therefore consider several model configurations for which the distributions can be found exactly. Moreover, we propose that the distributions that we consider give the maximal and the minimal possible weight to the low-energy Doppler shift, and therefore can be used to obtain the upper and the lower limits of the experimentally accessible quantities.

### A. Single vortex, $\mathbf{H}\|\hat{\mathbf{c}}$

The simplest of these models is that of a velocity field of an isolated vortex, cut off at the distance equal to the intervortex distance; since the experiments are in the dilute vortex limit such an approach gives an adequate description of the vortex state. The supervelocity is $\mathbf{v}_s(\mathbf{r})=\hbar\hat{\theta}/2mr$, where $\theta$ is the winding angle of the vortex in real space, $m$ is the effective mass, and $r$ is the distance from the center of the vortex. We now write the Doppler shift in terms of the energy scale $E_H=v_f/(2R)$, where $R$ is the radius of the unit cell of the vortex lattice, taken to be circular, $R=\sqrt{\Phi_0/\pi H}$ (Refs. 14,16),

$$\mathbf{v}_s(\mathbf{r})\cdot\mathbf{k}_f=\frac{\hbar k_f}{2mr}\sin\theta=\frac{E_H}{\rho}\sin\theta. \tag{22}$$

Here we have introduced the normalized length $\rho\equiv r/R$, and have chosen, without loss of generality, $\mathbf{k}_n$ along the direction $\theta=\pi/2$.

The probability distribution at a single node is now easily obtained from Eq. (18)

$$\begin{aligned}\mathcal{P}(\epsilon)&=\frac{1}{\pi}\int_0^{2\pi}d\theta\int_0^1\rho d\rho\,\delta\left(\epsilon-\frac{E_H}{\rho}\sin\theta\right)\\&=\frac{E_H^2}{\pi\epsilon^3}\int_0^{2\pi}d\theta\sin^2\theta\,\Theta\left(\frac{E_H}{\epsilon}\sin\theta\right)\Theta\left(1-\frac{E_H}{\epsilon}\sin\theta\right),\end{aligned} \tag{23}$$

yielding

$$\mathcal{P}(\epsilon)=\begin{cases}\dfrac{1}{2}\dfrac{E_H^2}{\epsilon^3}, & \text{if } \epsilon\geqslant E_H;\\[2ex] \dfrac{1}{\pi}\dfrac{E_H^2}{\epsilon^3}\left[\arcsin\dfrac{\epsilon}{E_H}-\dfrac{\epsilon}{E_H}\sqrt{1-\dfrac{\epsilon^2}{E_H^2}}\right], & \text{if } \epsilon<E_H.\end{cases} \tag{24}$$

Here we have taken $\epsilon\geqslant 0$, the probability density is even in $\epsilon$.

It was argued in Ref. 52 that the function $\mathcal{P}(\epsilon)$ for any vortex configuration has two important properties. First, the asymptotic behavior $\mathcal{P}(\epsilon)=E_H^2/(2\epsilon^3)$ holds for $\Delta_0\gg\epsilon\gg E_H$. Since the vortices repel each other, the vortex cores do not overlap. The large Doppler shifts come from the regions near the cores, where the superfluid velocity is high, and consequently are dominated by the single vortex physics. Second, in the absence of strong pinning $\mathcal{P}(\epsilon)$ has a single energy scale $E_H$ and depends on the Doppler shift only via $\epsilon/E_H$. Since the probability density is normalized,

$$\int_{-\infty}^{+\infty}\mathcal{P}(\epsilon)d\epsilon=1, \tag{25}$$

we can follow Ref. 52 and define a normalized dimensionless probability density as

$$P(x)=E_H\mathcal{P}(\epsilon/E_H), \tag{26}$$

where $x=\epsilon/E_H$.

The two-node probability distribution function is

$$\mathcal{L}(\epsilon_1,\epsilon_2)=\frac{1}{\pi}\int_0^{2\pi}d\theta\int_0^1\rho d\rho\,\delta\left(\epsilon_1-\frac{E_H}{\rho}\sin\theta\right)\times\delta\left(\epsilon_2-\frac{\epsilon_1\sin(\theta+\phi_0)}{\sin\theta}\right),\tag{27}$$

where $\phi_0$ is the angle between the nodes $\mathbf{k}_1$ and $\mathbf{k}_2$ at the Fermi surface. For the pure *d*-wave symmetry that we consider here, $\phi_0=\pi/2$, and the integral can be evaluated to give

$$\mathcal{L}(\epsilon_1,\epsilon_2)=\frac{1}{\pi}\frac{E_H^2}{(\epsilon_1^2+\epsilon_2^2)^2},\quad \text{if } \sqrt{\epsilon_1^2+\epsilon_2^2}\geqslant E_H,\tag{28}$$

and zero otherwise. The physical reason for the discontinuity is that for the nodes at the orthogonal positions $\epsilon_1^2+\epsilon_2^2=E_H^2/\rho^2\geqslant E_H^2$, so that the probability of having the Doppler shifts not satisfying this inequality is identically zero. In an orthorhombic system, where the nodes are not at angle $\pi/2$, the shape of the distribution is different. In analogy with the single-node probability density we can also define the dimensionless energies $(x,y)=(\epsilon_1,\epsilon_2)/E_H$, and introduce the function

$$L(x,y)=E_H^2\mathcal{L}(\epsilon_1,\epsilon_2)=\frac{1}{\pi(x^2+y^2)^2},\quad \text{if } x^2+y^2\geqslant 1,\tag{29}$$

and zero otherwise.

### B. Single vortex, H$\|\widehat{\mathbf{ab}}$

For the magnetic field applied in the superconducting plane it has been recently argued that for a relatively three-dimensional high-$T_c$ material, such as YBCO, the semiclassical approach still captures the essential features of the quasiparticle behavior.[17] The approach of Ref. 17 is to take the supervelocity field from an anisotropic London model, but to introduce the Doppler shift only in the dispersion of the quasiparticles with the momenta in the plane. After rescaling the *c* axis to make the unit cell of the vortex lattice isotropic, the Doppler shift is given by[17]

$$\mathbf{v}_s(\mathbf{r})\cdot\mathbf{k}_f=\frac{E_{ab}}{\rho}\sin\theta\sin(\phi-\alpha),\tag{30}$$

where the angle $\phi$ parametrizes the cylindrical Fermi surface, $\alpha$ is the angle between the direction of the magnetic field in the plane and the *x*-axis, and the in-plane energy scale is $E_{ab}=\eta E_H$, where in the London effective-mass model the anisotropy $\eta=(\lambda_{ab}/\lambda_c)^{1/2}$. In the nodal approximation (which provides an excellent agreement with the numerical results[17]) the probability distribution of the Doppler shift at a single node is given by Eq. (24) with $E_H$ replaced by $E_1=E_{ab}|\sin(\pi/4-\alpha)|$ and $E_2=E_{ab}|\cos(\pi/4-\alpha)|$, respectively, for the two pairs of nodes. Any effects of the three dimensionality reduce the effective value $E_{ab}$ rather severely,[17] so that the estimate obtained using the value of $\eta$ for the effective anisotropy in the two-dimensional case can only serve as an upper limit.

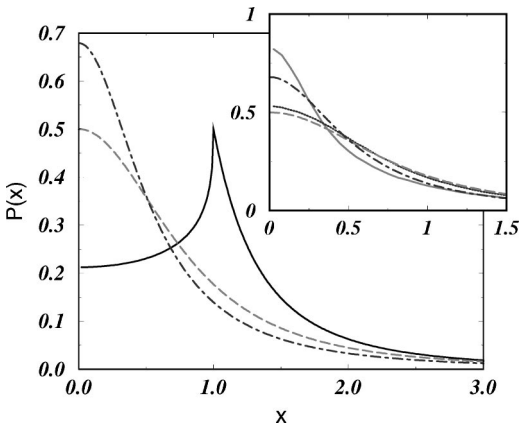


FIG. 1. Main panel: probability distribution $P(x)$ in the single-vortex approximation from Eq. (24) (solid line), and for a model vortex liquid states from Eq. (35) (dashed line) for liquid I model, and from Eq. (37) for the liquid II model (dot-dashed line). Inset: comparison of the distributions for the model liquid states (same notations as in the main panel) with the numerically determined distributions for pancake liquid in BSCCO at $T=9$ K (narrow distribution) and $T=67$ K (broad distribution) from Ref. 48.

For such a geometry the Doppler shifts at the two neighboring nodes are related by $\epsilon_2=E_2\epsilon_1/E_1$; in contrast to the case of the field applied along the *c* axis, the Doppler shift at one of the nodes uniquely determines the value of the Doppler shift at the other node independently of the winding angle $\theta$ in real space. Therefore the two-node probability distribution is given by

$$\mathcal{L}(\epsilon_1,\epsilon_2)=\mathcal{P}(\epsilon_1)\,\delta\left(\epsilon_2-\frac{E_2}{E_1}\epsilon_1\right),\tag{31}$$

and a single average is always sufficient for computing the physical quantities in the semiclassical approximations for the field applied in the plane.

### C. Vortex solids and liquids

We now discuss how the probability densities obtained above can be generalized to the case of vortex solids or liquids. We first consider the single-node probability density $P(x)$. Since this function is normalized, the question is what type of the redistribution of the density in Fig. 1 one may expect for realistic vortex structures. As argued above, the high-energy tail of the distribution is entirely determined by the single vortex physics, and is therefore insensitive to the structure of the vortex state; the redistribution of weight occurs in the region $x\lesssim 1$ or $\epsilon\lesssim E_H$.

It is also clear that the single vortex picture described above underestimates the number of points where the Doppler shift vanishes. For the supervelocity field of a single vortex $|\mathbf{v}_s(\mathbf{r})|>0$ everywhere in the unit cell, and the Doppler shift vanishes only for the superfluid velocity direction normal to the nodal directions in $\mathbf{k}$ space. In a vortex lattice there exist points where $|\mathbf{v}_s(\mathbf{r})|=0$: the high-symmetry locations such as midpoints between the centers of two neighboring vortices. Consequently, for vortex lattices $P(0)$ is larger than it is in the single-vortex picture. The weight shifted to

the vanishing Doppler shift, $x=0$, comes at the price of a reduction in the peak in $P(x)$ and moving the peak to smaller $x$. The actual shape of the function depends on the type of the vortex lattice, the number of nearest neighbors, and on relative orientation of the basis vectors of the vortex lattice with respect to the nodal directions.

As the number of nearest neighbors is increased, so is the value $P(0)$. This value depends not only on the number of zeros, but also on the asymptotic behavior of the supervelocity near a point where it vanishes, $v_s(\mathbf{r}_0)=0$. It is easy to check that if $v_s(\mathbf{r}-\mathbf{r}_0)\propto|\mathbf{r}-\mathbf{r}_0|^\nu$, the contribution of this area to $P(0)$ is finite for $\nu<2$, is singular but integrable for $2\leqslant\nu<3$, and is nonintegrable (and therefore nonphysical) for $\nu\geqslant 3$. In a typical vortex distribution $v_s$ varies linearly with the distance from $\mathbf{r}_0$, so that $P(0)$ remains finite. We now try to derive analytically an approximate distribution that gives a large weight to the probability of the vanishing Doppler shift; we consider it here to model a relatively disordered vortex state, such as a vortex liquid, and to provide a lower limit of the magnetic field dependence of the physical quantities. To make progress we consider a cylindrically symmetric spatial dependence of the supervelocity, modulated compared to the single-vortex distribution. Different choices for the modulation of the superfluid velocity are considered in the literature;[55,30] in any approach the supervelocity near the vortex core should remain nearly unmodified compared to the single-vortex velocity field, while at the cell boundary $v_s=0$. Therefore, in the cylindrically symmetric case, the Doppler shift (for $\mathbf{H}\|\hat{\mathbf{c}}$) can be approximated as

$$\mathbf{v}_s(\mathbf{r})\cdot\mathbf{k}_f=E_H S(\rho)\sin\theta, \tag{32}$$

where $S(\rho\to 0)\propto 1/\rho$ and $S(1)=0$.

Notice that the requirement that $P(0)$ is finite imposes restrictions on the decay of $S(\rho)$ as $\rho\to 0$. Since in the cylindrically symmetric model $v_s$ vanishes along a line rather than at discrete points (as it does for a realistic vortex distribution), the required asymptotic behavior of $S(\rho)$ is different from that of $v_s$ in the system with points of vanishing Doppler shift. Nevertheless, as we show below, the appropriate choice of $S(\rho)$ allows us to arrive at a probability distribution close to that obtained by numerical simulations of the vortex liquid. In such a liquid the distribution is temperature dependent. A detailed calculation therefore would have to take into account the changes in the probability density with the temperature in a given material. These changes are not well understood beyond simple models, and even then are usually accessible only via numerical simulations of the vortex dynamics. We therefore take the point of view that for a qualitative or semiquantitative analysis it is sufficient to consider a model temperature-independent distribution.[52]

Computing the distribution $\mathcal{P}(\epsilon)$ from Eq. (18) we obtain

$$P(x)=\frac{1}{\pi}\int_0^1\frac{\rho d\rho}{\sqrt{S^2(\rho)-x^2}}. \tag{33}$$

Clearly, $P(0)$ is finite when $S(\rho\to 1)\propto(1-\rho)^\eta$ with $\eta<1$. We use here two different models where the superfluid velocity field of a single vortex is modulated to vanish at the unit cell boundary in a fashion that allows analytical progress. In the first, we take the modulating factor to be $(1-r^2/R^2)^{1/2}$, which leads to $S(\rho)=\sqrt{1-\rho^2}/\rho$. Computing the probability densities as in the previous section we find

$$\mathcal{L}(\epsilon_1,\epsilon_2)=\frac{1}{\pi}\frac{E_H^2}{(\epsilon_1^2+\epsilon_2^2+E_H^2)^2}, \tag{34}$$

and

$$\mathcal{P}(\epsilon)=\frac{1}{2}\frac{E_H^2}{(E_H^2+\epsilon^2)^{3/2}}. \tag{35}$$

In this case the measure of Doppler shift zeros is large due to disorder in the positions of vortices, $P(0)=0.5$. The simplicity of this probability distribution makes this choice attractive for further analytical work.

Another possible choice is $S(\rho)=\sqrt{1-\rho}/\rho$; it leads to

$$\mathcal{L}(\epsilon_1,\epsilon_2)=\frac{1}{\pi}\frac{E_H^4}{(\epsilon_1^2+\epsilon_2^2)^3}\times\left\{1+\frac{\epsilon_1^2+\epsilon_2^2}{E_H^2}-\frac{1}{\sqrt{4\dfrac{\epsilon_1^2+\epsilon_2^2}{E_H^2}+1}}\left[1+3\frac{\epsilon_1^2+\epsilon_2^2}{E_H^2}\right]\right\}. \tag{36}$$

Note that as $(\epsilon_1^2+\epsilon_2^2)E_H^2\to 0$ the distribution $\mathcal{L}$ is finite: $\mathcal{L}(0,0)=2/(\pi E_H^2)$. The corresponding single-node probability density is given by

$$\mathcal{P}(\epsilon)=\frac{1}{\pi E_H}\left\{\left[\frac{E_H^3}{\epsilon^3}+\frac{3E_H^5}{4\epsilon^5}\right]\arccos\frac{1}{\sqrt{(2\epsilon/E_H)^2+1}}-\frac{3E_H^4}{2\epsilon^4}\right\}. \tag{37}$$

For this distribution $P(0)=32/(15\pi)\approx 0.68$, larger than the value of 0.5 given by Eq. (35).

The probability density $P(x)$ for all three distributions is shown in Fig. 1. In the following we will refer to the distributions given by Eqs. (34) and (35) and by Eqs. (36) and (37) as liquid I and liquid II, respectively. The reason for that is clear from the inset of Fig. 1: these distributions are close to those obtained with the help of the Langevin dynamics simulations of the pancake liquid in Ref. 52; as in the vortex liquid they preserve the cylindrical symmetry of the supervelocity field on average, while introducing zeros in that field because of the cancellation of the supervelocity from neighboring vortices. For a realistic vortex lattice we expect the results for thermodynamic quantities to be bracketed by the values obtained in the single vortex approach, which overestimated the effect of the field by undercounting the number of points in the unit cell of the vortex lattice where the Doppler shift for quasiparticles near a particular node vanishes, and, at least approximately, by the liquid II distribution given by Eqs. (36) and (37). The distribution function for the pancake liquid can be even sharper peaked at $x=0$;

nevertheless, we believe that the approximate analytic form provides a reasonable low-end estimate for most of the experimental situations.

### D. Completely disordered vortex state

The ''universal'' high Doppler shift behavior of the probability density, $P(x) \propto x^{-3}$ results from the strong repulsion between the vortex lines that prevents vortex cores from overlapping. If the vortices were noninteracting, in a disordered state their positions would be completely random, leading to a Gaussian distribution of the Doppler shifts. Such an approximation has been used by Yu *et al.*[54] and Franz[50] in their analysis of the thermal conductivity in the vortex state. Even though it is never realized, it is instructive to compare the predictions obtained with such a distribution with the results obtained in the framework outlined above. The comparison may be useful for the extremely anisotropic layered superconductors in the geometry with the field applied in the basal plane. In that arrangement vortices lack proper cores, the intervortex repulsion is weakened, and we expect significant disorder in vortex positions due to the presence of defects (such as boundary effects, twin boundaries, etc.). Consequently, the $1/x^3$ asymptotic behavior does not onset up to large Doppler shifts (very close to the core), and over the low (compared to the gap amplitude) energies, the probability density decays rapidly. We therefore also consider in the following the random distribution of vortices, which leads (omitting factors of $\ln \lambda_L/\xi_0$ in the width of the Gaussian) to the probability density[54,50]

$$P(x) \approx \frac{1}{\sqrt{\pi}} e^{-x^2}. \tag{38}$$

We now investigate the dependence of the thermodynamic coefficients on the magnetic field and the temperature for different structure of the vortex state and compare it with the experimentally observed behavior.

## V. DENSITY OF STATES: PURE LIMIT

We begin by considering the density of states and the electronic contribution to the specific heat in the pure limit. While this is one of the simplest quantities to analyze, it is the one directly relevant to the measurements of the field dependence of the specific heat in YBCO single crystals.[2–5] To justify ignoring impurities in this analysis we emphasize that the energy scales associated with the Doppler shift are quite large, and at moderate fields exceed the impurity bandwidth even in not too clean samples, and exceed it by far in the latest single crystals.[4,5] Taking the Fermi velocity $v_f \sim (1.5-2.5)\times 10^7$ cm/s,[33] we obtain $E_H/\sqrt{H} \sim 30$ K T$^{-1/2}$, and for YBCO near optimal doping, where $1/\eta \sim 2.5-4$, we obtain $E_{ab}/\sqrt{H} \leqslant 10$ K T$^{-1/2}$, while the impurity bandwidth $\gamma$ is of the order of a few kelvin or less.

### A. Density of states for $\mathbf{H} \| \hat{\mathbf{c}}$

We first consider the experimental arrangement with $\mathbf{H} \| \hat{c}$. The density of states in the pure limit is given by Eq. (17) leading to

$$N(\omega,H) = \int_{-\infty}^{+\infty} d\epsilon N(\omega+\epsilon)\mathcal{P}(\epsilon) = \int_{-\infty}^{+\infty} d\epsilon \frac{|\omega+\epsilon|}{\pi v_f v_\Delta}\mathcal{P}(\epsilon). \tag{39}$$

Introducing the dimensionless variable $x=\epsilon/E_H$ and considering hereafter $\omega \geqslant 0$ we find that the density of states is given by

$$N(\omega,H) = \frac{2\omega}{\pi v_f v_\Delta}\int_0^{\omega/E_H} P(x)dx + \frac{2E_H}{\pi v_f v_\Delta}\int_{\omega/E_H}^{\infty} xP(x)dx. \tag{40}$$

The scaling properties of the density of states with $\omega/E_H$ (Ref. 56) can be made obvious by rewriting it as

$$N(\omega,H) = \frac{E_H}{\pi v_f v_\Delta} F_N\left(\frac{\omega}{E_H}\right), \tag{41}$$

$$F_N(Z) = 2\left(Z\int_0^Z P(x)dx + \int_Z^\infty xP(x)dx\right). \tag{42}$$

The residual density of states at the Fermi surface is given by

$$N(0,H) = M_1 \frac{E_H}{\pi v_f v_\Delta} = \frac{M_1}{2v_\Delta}\sqrt{\frac{H}{\pi\Phi_0}}, \tag{43}$$

where $M_1$ is the first moment of the probability distribution of the Doppler shift

$$M_1 = 2\int_0^\infty xP(x)dx, \tag{44}$$

which contains all the information about the structure of the vortex state relevant to the magnitude of the $\sqrt{H}$ term in the specific heat. For the probability density given by Eq. (24) (single-vortex model) we then find $M_1^s = 4/\pi \approx 1.27$, while for the liquid I distribution given by Eq. (35) we obtain $M_1^l = 1$. For liquid II distribution the integral can be evaluated numerically to give $M_1^{l2} \approx 0.85$, while for the completely disordered distribution of vortices $M_1^g = 1/\sqrt{\pi} \approx 0.56$. We therefore expect that $M_1 \sim 1$ for any realistic vortex state. Furthermore, since the number of zeros of the Doppler shift increases with the increased disorder in the lattice,[52] we expect on general grounds that the coefficient is larger for the more ordered vortex state. The residual density of states given by Eq. (43) is close to the expression obtained by Won and Maki in a different approximation scheme.[57]

Expanding Eqs. (41) and (42) at low energies $\omega \ll E_H$ we find

$$N(\omega,H)\approx\frac{E_H}{\pi v_f v_\Delta}\left(M_1+\frac{\omega^2}{E_H^2}P(0)\right). \tag{45}$$

Therefore the energy dependence of the density of states in the field-dominated regime is determined by the probability weight of the vanishing Doppler shift. As the lattice changes toward a larger coordination number and toward disorder, the measure of points where the superfluid velocity vanishes increases. As a result, the coefficient of the leading field-dependent term $M_1$ decreases, while the coefficient of the energy-dependent term $P(0)$ increases. The values of this coefficient are $P^s(0)=2/3\pi\approx0.21$, $P^l(0)=0.5$, $P^{l2}(0)=0.68$, and $P^g(0)=1/\sqrt{\pi}\approx0.56$ for the single vortex, liquid I, liquid II, and Gaussian distributions, respectively. It immediately follows that the position of the crossover from the field-dominated to the zero-field temperature-dominated behavior in the average density of states is much more sensitive to the structure of the vortex state than the leading field-dependent term.

In the effective weak-field range, $\omega\gg E_H$, the field-dependent contribution is independent of the distribution of vortices. The vortices are well separated, and the regions where the Doppler shift exceeds the temperature are close to the cores, and consequently dominated by the universal tails $P(x)=1/2x^3$, yielding

$$N(\omega,H)\approx\frac{\omega}{\pi v_f v_\Delta}\left(1+\frac{1}{2}\frac{E_H^2}{\omega^2}\right). \tag{46}$$

The full dependence of the density of states on the energy and the magnetic field can be obtained from Eqs. (41) and (42) with the probability densities discussed above. For the single-vortex picture we regain the result of Kübert and Hirschfeld[14]

$$F_N^s(Z)=\frac{Z}{\pi}\begin{cases}\pi(1+Z^{-2}/2), & \text{if } Z\geqslant 1;\\ Z^{-2}[(1+2Z^2)\arcsin Z+3Z\sqrt{1-Z^2}], & \text{if } Z\leqslant 1.\end{cases} \tag{47}$$

For the liquid I model we obtain a remarkably simple result

$$F_N^l=\sqrt{Z^2+1}, \tag{48}$$

$$N^l(\omega,H)=\frac{\sqrt{\omega^2+E_H^2}}{\pi v_f v_\Delta} \tag{49}$$

while for the liquid II model the integral can only be evaluated numerically, and for the Gaussian model

$$F_N^g(Z)=Z\Phi(Z)+\frac{\exp(-Z^2)}{\sqrt{\pi}}, \tag{50}$$

where $\Phi(Z)$ is the probability integral.[58] Notice that for the Gaussian distribution the enhancement of the density of states in the weak field limit, $\omega\gg E_H$ is vanishingly small in $\omega/E_H$, in contrast to Eq. (46). Indeed, in this limit the field-dependent part of the density of states is determined by the weight in the part of the distribution $\mathcal{P}(\epsilon)$ with $\epsilon\geqslant\omega$, which is exponentially small.

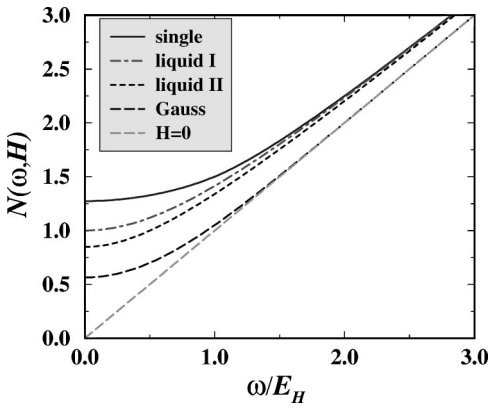


FIG. 2. Energy dependence of the density of states in the magnetic field for different models of the probability density for the Doppler shift. Density of states is in units of $E_H/(\pi v_f v_\Delta)$.

This difference is clear from Fig. 2. The low energy limit of the density of states depends on the moment of the distribution function, and is therefore different for each of the model distributions. On the other hand the high energy, or weak field, limit yields the same result for the models respecting the asymptotic $x^{-3}$ decay for the probability distribution $P(x)$, while the Gaussian model gives the density of states which is not enhanced relative to the zero-field value. The Gaussian model therefore misses the field-dependent contribution to the physical quantities at high energies, leading to incorrect results, especially in the regime $T\leqslant E_H$.

### B. Density of states for H$\|\widehat{\mathbf{ab}}$

We can now analyze in the same framework the anisotropy in the density of states for the field applied in the superconducting plane, at an angle $\alpha$ to the $x$ axis. As discussed in Sec. IV B, density of states for such a configuration is a sum over the two inequivalent pairs of nodes, with the different characteristic scales for the Doppler shift at each pair of nodes,

$$E_1=E_{ab}|\sin(\pi/4-\alpha)|, \tag{51}$$

$$E_2=E_{ab}|\cos(\pi/4-\alpha)|. \tag{52}$$

In the London model $E_{ab}=\eta E_H$, where $\eta$ is the penetration depth anisotropy ratio. We emphasize that in reality the value of the ''effective'' anisotropy depends on the details of the $c$-axis transport properties,[17] and therefore the estimate of $E_{ab}/\sqrt{H}\sim10\ \mathrm{K\,T^{-1/2}}$ is just an upper limit on its magnitude, and, as we comment below, the value inferred from the available experimental data on the specific heat is lower.

The density of states in the clean limit is given by

$$N(\omega,H;\alpha)=\tfrac{1}{2}[N_1(\omega,H)+N_2(\omega,H)], \tag{53}$$

where $N_i$ is computed from Eq. (41) as in the previous section but with $E_i$ $(i=1,2)$ replacing $E_H$.

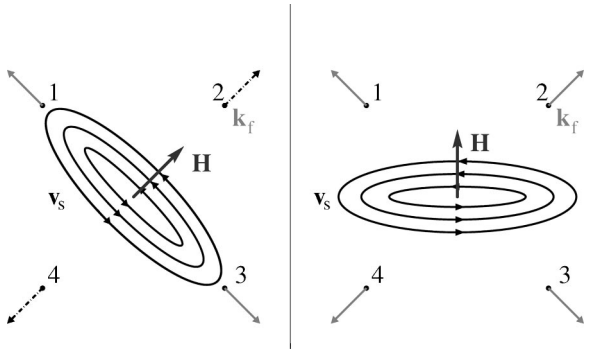


FIG. 3. Contribution of different nodes to the density of states. The nodes are numbered and the direction of the Fermi momentum is shown at each nodal point. Left: field along the nodal direction and orthogonal to the other pair of nodes. The Fermi momentum at nodes 2 and 4 (broken line) is orthogonal to the plane where supercurrents flow, and the Doppler shift vanishes everywhere in space for this pair of nodes. Right: field in the antinodal direction. The Doppler shift is nonvanishing at some points in space for each node, and the density of states is maximal.

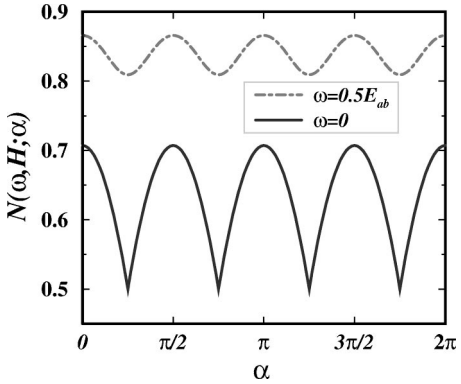


FIG. 4. Angular dependence of the density of states, measured in units of $E_{ab}/(\pi v_f v_\Delta)$, on the the direction of the applied magnetic field. Density of states has been computed with the model liquid I probability density of the Doppler shift. Angle $\alpha$ is measured with respect to the $x$ axis, and the minima are along the position of the nodes. Notice a significant reduction in the anisotropy at energies of the order of $E_{ab}$.

As is known[17,19] the residual density of states exhibits fourfold oscillations as a function of the direction of the applied field in the plane

$$N(0,H;\alpha)=\frac{M_1}{2}\frac{E_1+E_2}{\pi v_f v_\Delta}=\frac{M_1}{\sqrt{2}\pi}\frac{E_{ab}}{v_f v_\Delta}\max[|\sin\alpha|,|\cos\alpha|]. \tag{54}$$

The minima of the density of states occur when the field is along the nodal direction, $\alpha=\pi/4+\pi n/2$. In that case at two of the four nodes the circulating currents are in the plane orthogonal to the direction of the Fermi momentum at the node, and consequently the Doppler shift vanishes at all points in real space (either $E_1=0$ or $E_2=0$), as seen in Fig. 3. In contrast, when the field is along the antinodal direction, the Doppler shift in non-zero, and all four nodes contribute to the density of states, leading to a maximum in $N(\omega,H)$.[17] It is important to emphasize that, as is clear from Fig. 3, it is only for a tetragonal system that the minima in the density of states occur for the field along the node. One reason for that is that in an orthorhombic system ($m_a\neq m_b$), for the field applied in a direction other than along the principal axes of the effective mass tensor, the directions of the internal and the external fields differ.[59] The difference may be quite small in the experimentally relevant field range; ignoring it, Schachinger and Carbotte[60] argued that the minima occur when the field is parallel to the direction of the Fermi velocity at the node, which differs from the direction toward the node.

The anisotropy in the density of states given by Eq. (54) is $\sim 30\%$ for the purely two-dimensional model considered here. Any three-dimensionality reduces this number severely: if there is a line of nodes extending along the $z$ axis, for the field applied toward a node in the equatorial plane, the Doppler shift vanishes only for the nodal quasiparticles with momenta in the plane. For the quasiparticles on the same nodal line but with a component of the momentum along the $z$ axis the Doppler shift is finite, consequently the node is still ''active'' in contributing to the density of states. In the simplest estimate in a three-dimensional system[17] the effect is reduced to 7–8 %, in some models with a tight-binding dispersion[61] along the $c$ axis it may be reduced even further, to about 4%, making the effect more difficult to detect.

The anisotropy is also rapidly washed out with increased energy.[17] Since the density of states has a minimum when the field is applied along a node ($E_1=0$ for example), the corresponding pair of nodes is ''inactive'' and insensitive to the field; therefore the density of states increases linearly in energy, as in the absence of a field. For the field away from the nodal direction the density of states increases as a square of the energy, see Eq. (45), resulting in a rapid suppression of the difference between the two geometries. For low energies in the limit $\omega\ll E_1,E_2$, which can only happen if the field is not close to a nodal direction ($E_1,E_2\neq 0$), we have

$$N(\omega,H;\alpha)\approx\max[|\sin\alpha|,|\cos\alpha|]\frac{E_{ab}}{\pi\sqrt{2}v_f v_\Delta}\times\left[M_1+\frac{\omega^2}{E_{ab}^2}\frac{2}{|\cos 2\alpha|}P(0)\right]. \tag{55}$$

On the other hand, if $E_1\ll\omega\ll E_2$, which may happen when the field is close to one of the nodes, and $E_1\ll E_2$, we have

$$N(\omega,H;\alpha)\approx\frac{1}{2\pi v_f v_\Delta}\left[M_1E_2+\omega+\frac{\omega^2}{E_2}P(0)+\frac{E_1^2}{2\omega}\right]. \tag{56}$$

The anisotropy in the density of states as a function of the angle for the liquid I model is shown in Fig. 4, at low energies there is no qualitative difference between the different models, see below. As the energy is increased the sharp minima fill up, and the resulting anisotropy decreases.

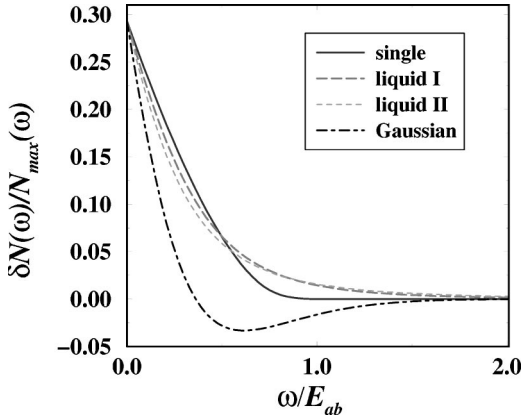


FIG. 5. Relative anisotropy in the density of states, $\delta N(\omega) = N(\omega,H;\alpha=0) - N(\omega,H;\alpha=\pi/4)$ normalized by the maximal $N_{max}(\omega)=N(\omega,H;0)$ for different models considered in the text. Notice that the relative anisotropy at $\omega=0$ is identical for all models, as is clear from Eq. (54). In the single-vortex model the anisotropy vanishes identically at $\omega \geqslant E_{ab}$, see Eq. (47). For the Gaussian model the exponential asymptotic behavior of the probability distribution leads to the inverse anisotropy in the intermediate energy range. The two liquid models yield a very similar dependence of the anisotropy on the energy.

The angular dependence of the density of states vanishes at higher energies, as for $\omega \gg E_1, E_2$ with a realistic distribution respecting the asymptotic behavior $P(x) \propto x^{-3}$ for $x \gg 1$

$$N(\omega,H;\alpha) \approx \frac{\omega}{\pi v_f v_\Delta}\left(1+\frac{1}{4}\frac{E_1^2+E_2^2}{\omega^2}\right) = \frac{\omega}{\pi v_f v_\Delta}\left(1+\frac{1}{4}\frac{E_{ab}^2}{\omega^2}\right). \quad (57)$$

The exact crossover scale from the strong- to the weak-field regime depends on the particular choice of the probability distribution. This is shown in Fig. 5 for the three different choices of $P(x)$ considered in this work.

### C. Zeeman splitting

Typically the Zeeman shift is small compared to the Doppler energy scale, and does not modify significantly the density of states. Indeed, for the field along the *c*-axis, the spin-up and spin-down density of states is given by

$$N^{\pm}(\omega,H) = \frac{E_H}{\pi v_f v_\Delta} F_N\left(\frac{\omega_\pm}{E_H}\right), \quad (58)$$

where $\omega_\pm = |\omega \pm \mu H|$. Therefore, for example, the corrections to the residual density of states due to the paramagnetic contributions in the regime $\mu H \ll E_H$ are of the order

$$\frac{\delta N(0,H)}{N(0,H)} \approx \left(\frac{\mu H}{E_H}\right)^2 \frac{P(0)}{M_1} \ll 1. \quad (59)$$

For quasi-three-dimensional materials, such as YBCO, the relevant energy for the field applied in the plane is $E_{ab}$. Even if this energy scale is only 15% of $E_H$, a factor of 2–3 smaller than estimated, the ratio $E_{ab}/\mu H \sim 6.7/\sqrt{H\ \mathrm{T}^{1/2}}$ implies a crossover field of 45 T. Consequently the Zeeman splitting is unimportant compared to the Doppler shift in the experiments performed so far in YBCO. This is in contrast to more two-dimensional materials, such as BSCCO, where the response to a parallel magnetic field is dominated by the Zeeman splitting.[63,64]

The situation is different for the geometry with the field applied along a node; this was first pointed out in Ref. 20. In this case the Doppler shift at one pair of the nodes vanishes, and, at $\omega=0$, the only contribution to the density of states at these nodes is due to the Zeeman splitting. The Zeeman splitting leads to a finite contribution to the density of states that is linear in $\mu H$, and consequently reduces the residual anisotropy $\delta N(0,H)$. This reduction has been investigated in Ref. 20.

This is, however, not the only effect of the paramagnetic coupling. Since the density of states at the nodes with the vanishing Doppler shift is now dominated by the Zeeman splitting at low energies, the anisotropy is not reduced as rapidly with the increasing energy. Indeed, if only the paramagnetic effect is taken into account, the total (per particle, i.e. summed over the spins rather than per spin) density of states is

$$N_Z(\omega,H) = \sum_{\alpha=\pm} \frac{|\omega+\alpha\mu H|}{\pi v_f v_\Delta} = \frac{2\max[\mu H,|\omega|]}{\pi v_f v_\Delta}, \quad (60)$$

and therefore the anisotropy increases with $\omega$ up to $\omega = \mu H$, where it reaches a maximum.

Let us consider the liquid I model, where the analytic expression for the density of states is particularly simple, the results are not modified substantially if other models are used. The anisotropy in the total (summed over the spin directions) density of states between the nodal and the antinodal directions is given by

$$\delta N(\omega,H) = \frac{1}{2\pi v_f v_\Delta}\left[\sum_{\alpha=\pm}\left(2\sqrt{\omega_\alpha^2+E_{ab}^2/2}-\sqrt{\omega_\alpha^2+E_{ab}^2}\right) - 2\max[\mu H,|\omega|]\right] \quad (61)$$

As Fig. 6 demonstrates, even though the zero-energy anisotropy is severely reduced upon inclusion of the Zeeman splitting, the anisotropy at moderate energies is close to the result obtained without accounting for the paramagnetic effect. It is clear that the magnitude of the reduction and the crossover energy depend on the actual value of $E_{ab}$, and we need a realistic estimate of this value to evaluate the impact of the paramagnetic splitting on the experimental results for the field along a nodal direction. Such an estimate can be obtained from the analysis of the data on the specific heat that we discuss in the next section.

## VI. SPECIFIC HEAT AND SCALING

The information about the density of states is experimentally available primarily via the specific-heat measurements,

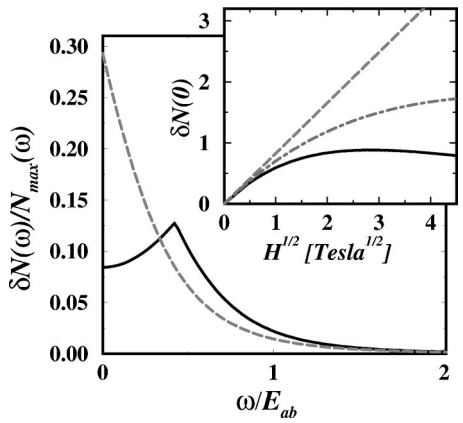


FIG. 6. Effect of the Zeeman splitting on the anisotropy in the density of states. Here $E_{ab}/\sqrt{H}=a$ K T$^{-1/2}$. Main panel: energy dependence of the anisotropy for the liquid I distribution with (solid line) and without (dashed line) accounting for the Zeeman splitting for $a=5$ at $H=10$ T. Inset: anisotropy in the residual density of states, in units of $a/2\pi v_f v_\Delta$, as a function of the applied field. Dashed line: no Zeeman effect, dot-dashed line: $a=10$, solid line: $a=5$.

and we now address this quantity in more detail. The preliminary analysis of some of these issues within the single-vortex picture has been carried out by us before.[62] Here we concentrate on the effects of different distributions, and on the measurability of the specific heat anisotropy.

### A. Specific heat

The electronic contribution to the specific heat is given by[14,62]

$$C(T,H)=\frac{1}{2}\int_{-\infty}^{+\infty}d\omega N(\omega,H)\left(\frac{\omega^2}{T^2}\right)\cosh^{-2}\frac{\omega}{2T}$$

$$=T\int_0^\infty dx x^2 N(xT,H)\cosh^{-2}\frac{x}{2}. \qquad (62)$$

Making use of Eq. (41) we can rewrite the specific heat in the form useful for further analysis. For the field along the $c$ axis, $\mathbf{H}\|\hat{\mathbf{c}}$, we have

$$C(T,H)=\frac{TE_H}{\pi v_f v_\Delta}\int_0^\infty dx x^2 F_N\left(\frac{xT}{E_H}\right)\cosh^{-2}\frac{x}{2}, \qquad (63)$$

where $F_N$ is given by Eq. (42).

As a result we find in the limit $E_H \gg T$

$$C(T,H)\approx\frac{2TE_H}{\pi v_f v_\Delta}\left(\frac{\pi^2}{3}M_1+\frac{7\pi^4}{15}P(0)\frac{T^2}{E_H^2}\right), \qquad (64)$$

and in the opposite limit, $E_H \ll T$,

$$C(T,H)\approx\frac{2T^2}{\pi v_f v_\Delta}\left(9\zeta(3)+\frac{E_H^2}{T^2}\ln 2\right). \qquad (65)$$

Two quantities that can be compared with experiment are the coefficient of the $T^2$ term in absence of the field,

$$\gamma_s=\frac{k_B^3}{\hbar^2}\frac{nV_{mol}}{s}\frac{18\zeta(3)}{\pi v_f v_\Delta}, \qquad (66)$$

and the coefficient of the $T\sqrt{H}$ term at low temperature

$$p=\lim_{T\to 0}\frac{C(T,H)}{T}=\frac{\pi^{3/2}}{3}\frac{k_B^2}{\hbar}\frac{nV_{mol}}{s}\frac{M_1}{v_\Delta\Phi_0^{1/2}}. \qquad (67)$$

Here $V_{mol}$ is the molar volume, $s$ is the unit cell size along the $c$ axis, and $n$ is the number of $CuO_2$ layers per unit cell. The presence of both terms has been firmly established from the analysis of the experimental data on the specific heat in YBCO,[2,3,5] however, there remains disagreement about the values of the coefficients between different groups.

For that material $V_{mol}=104.6$ cm$^3$/mol, $n=2$, and $s\approx 12$ Å . The coefficient $p$ can in general be determined to a higher degree of accuracy, and the values available in the literature are $p\approx 0.91$ (mJ mol$^{-1}$/K$^2$) T$^{-1/2}$ for moderately clean samples,[2,3] and more recently obtained $p\approx 1.34$ (mJ mol$^{-1}$/K$^2$) T$^{-1/2}$ for the ultrapure single crystals.[5] The analysis of these data in the single-vortex picture has been carried out by Wang *et al.*,[5] and by Chiao *et al.*[40] In that picture the 50% difference in the coefficient translates into the same relative difference in the value for the slope of the gap. In contrast, according to the previous section, the more ordered vortex state leads to a larger first moment of the distribution, and consequently to a larger value of $p$ in Eq. (67); it is therefore reasonable that a higher-quality crystal would have a more ordered vortex state and hence a larger coefficient $p$. If we set $M_1=1$ the experimental values of $p$ lead to the values for the slope of the gap of $v_\Delta\approx 1.5\times 10^6$ cm/s and $v_\Delta\approx 1.0\times 10^6$ cm/s, respectively. On the other hand, $M_1=4/\pi$ for the pure crystal yields a larger $v_\Delta\sim 1.27\times 10^6$ cm/s, leading to a less than 20% discrepancy between the groups. The disagreement can be further reduced by assuming a disordered state with $M_1<1$ in the ceramic sample of Ref. 3. We also note that the pure crystal of Ref. 5 is overdoped, rather than optimally doped as in the work of Refs. 2 and 3, which may contribute to the difference in the coefficient. In combination with the value for the ratio $v_f/v_\Delta\approx 14$ obtained from the universal limit of the thermal conductivity[65] this yields $v_f\sim 1.8\times 10^7$ cm/s. This is in reasonable agreement with the value of the Fermi velocity obtained from the ARPES measurements in BSCCO,[33] which is believed to have a Fermi surface similar to that of YBCO.

The coefficient $\gamma_s$ of the temperature dependence has been measured with significantly larger error bars, and the results from different groups vary significantly: Moler *et al.*[2] reported the value of 0.1 (mJ mol$^{-1}$) K$^{-3}$, Wright and co-workers[3] obtained $\gamma_s\sim 0.064$ in the same units, while Wang *et al.*[5] measured 0.21. From the comparison with Eq. (66) we find $v_f v_\Delta\sim a\times 10^{13}$ cm$^2$/s$^2$, where $a=2.9,4.5,1.4$ for the three values given above. All these yield the Fermi velocity within a factor of two of the estimate given above. This implies that in the calculations requiring a cutoff in energy the cutoff $E_0\sim(1.3-2.3)\times 10^3$ K.

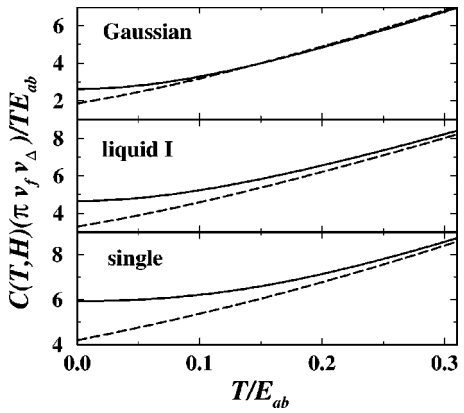


FIG. 7. Anisotropy in the specific heat between the nodal (dashed line) and antinodal (solid line) directions for different models.

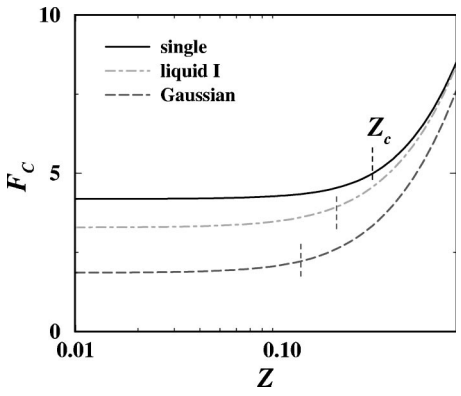


FIG. 8. Scaling function for the specific heat. For concreteness the crossover values $Z_c$ have been defined as the point of a 20% increase above the high-field flat region: $F_C(Z_c)=1.2F_C(0)$.

We now turn our attention to the field applied in the $ab$ plane, and discuss the specific heat following the general approach of our previous paper.[62] The first question that we address is the observability of the fourfold oscillations in the density of states. These oscillations have not been seen in the experiments by Moler *et al.*;[2] nor have they been found in recent measurements on very high quality single crystals of YBCO.[5] It seems likely that the estimate of $E_{ab}\sim 10\ \mathrm{K\,T^{-1/2}}$ from the purely two-dimensional model is too high, and the three-dimensionality reduces the effect significantly.[17] It is also possible that the orthorhombicity, which shifts the minima in the density of states away from the $\pi/4$ directions, combined with twinning of the crystals used in both experiments reduces the observable anisotropy significantly.[60] However, even in this case, the in-plane anisotropy for the fields of up to 14 T used in the experiments by Wang *et al.*[5] should be within the experimental resolution. A very important observation is that since the anisotropy in the density of states is washed out rapidly as the energy is increased, the in-plane anisotropy of the specific heat is greatly reduced with increased temperature,[17] as seen in Fig. 7 the reduction is more rapid for the Doppler shift density with the larger weight at low energies. We only consider here the possible situation when the configuration of the vortex lattice is identical for the field along the nodal and the antinodal directions; then the limiting behavior for the specific heat with the field along an antinode ($\alpha=0$) and along a node ($\alpha=\pi/4$) is easily obtained from Eqs. (55) and (56),

$$C(T,H;0)=\frac{\sqrt{2}E_{ab}T}{\pi v_f v_\Delta}\left[\frac{\pi^2}{3}M_1+\frac{14\pi^4}{15}\frac{T^2}{E_{ab}^2}P(0)\right], \quad (68)$$

$$C\left(T,H;\frac{\pi}{4}\right)=\frac{E_{ab}T}{\pi v_f v_\Delta}\left[\frac{\pi^2}{3}M_1+9\zeta(3)\frac{T}{E_{ab}}\right]. \quad (69)$$

Therefore while the amplitude of the $\sqrt{H}$ term confirms the estimates for the nodal velocities $v_f$ and $v_\Delta$, and therefore for the energy scale $E_H$, such a term has not been observed for the field in the plane, and therefore there is no direct measurement of $E_{ab}$ available. However, an estimate for this scale can be obtained from the scaling plots for the specific heat.

### B. Scaling functions

It has been pointed out by Simon and Lee[56] that on general grounds the thermodynamic coefficients of the nodal fermions in a magnetic field should scale with the variable $T/E_H$; consequently the experimental results can be interpreted as giving the form of these scaling functions. The scaling of the specific heat itself follows easily from Eq. (41) for the density of states, and the weak and the strong-field limits of the scaling function are obtained from the equations for the specific heat above. For the field $\mathbf{H}\|\hat{\mathbf{c}}$, we define $Z=T/E_H$ and $F_C(Z)=\pi v_f v_\Delta C(T,H)/(2TE_H)$; then

$$F_C(Z)=\int_0^\infty dx x^2 F_N(xZ)\cosh^{-2}\frac{x}{2}, \quad (70)$$

with $F_N$ given by Eq. (42). The limits for the scaling function follow easily:

$$F_C(Z)=\begin{cases}\pi^2 M_1/3+7\pi^4 P(0)Z^2/15, & \text{if } Z\ll 1;\\ 9\zeta(3)Z+Z^{-1}\ln 2, & \text{if } Z\gg 1.\end{cases} \quad (71)$$

The numerically determined scaling function is shown in Fig. 8. It is remarkably similar to the scaling plot obtained from the measured specific heat in Ref. 3. In that experiment the crossover scale, marking the transition from the field-dominated regime, where $F_C(Z)\approx$const, to the temperature dominated regime, has been determined to be $T/\sqrt{H}\approx 6.5$ $\mathrm{K/T^{1/2}}$; a very close value has been obtained in a more recent experiment of Wang *et al.*[5] As is clearly seen from Fig. 8 the value of the scaling variable at the crossover depends on the structure of the vortex state; this is easy to understand from Eq. (71). The zero temperature value of the scaling function is determined by the first moment of the Doppler shift distribution $M_1$, while the increase of $F_C$ with the temperature is proportional to the weight of the distribution at the vanishing Doppler shift $P(0)$. Consequently the crossover value $Z_c$ can be expected to be proportional to $\sqrt{M_1/P(0)}$. As the

number of zeros of the superfluid velocity grows, the weight in $P(x)$ is shifted toward lower energies, so that $M_1$ decreases while $P(0)$ increases; these opposing trends lead to significant variations in $Z_c$. From Fig. 8, for the liquid and single-vortex models the crossover occurs around $Z_c \simeq 0.2-0.3$; taking this value as the experimentally determined crossover point, we arrive at $E_H/\sqrt{H} \sim 30$ K T$^{-1/2}$, in agreement with our previous estimate. Notice that the crossover occurs at $Z_c \ll 1$; this is simply the result of a large coefficient of the $Z^2$ term in the low-temperature expansion in Eq. (71), $7\pi^4/15 \simeq 45$, while $\pi^2/3 \simeq 3$.

A similar analysis can be carried out for the field applied in the plane by introducing $Z_{ab}=T/E_{ab}$ and $F_{ab}(Z_{ab};\alpha) = \pi v_f v_\Delta C(T,H;\alpha)/(TE_{ab})$; the limiting form of the scaling functions for $Z_{ab} \ll 1$ can be read off Eqs. (68) and (69); at $Z_{ab} \gg 1$ we have

$$F_{ab} = 18\zeta(3) Z_{ab} + Z_{ab}^{-1} \ln 2. \tag{72}$$

The specific-heat data of Refs. 2 and 3 are analyzed by modeling and subtracting the ''background'' contributions to the specific heat (phonons, Schottky anomalies, etc.). To avoid the extensive analysis, Revaz *et al.*[4] have looked at the difference between the specific heat with the field along the *c* axis, and the field along the antinodal direction, the $c/a-b$ difference $\delta C(T,H) = C(T,H) - C(T,H;0)$. The comparison between the results of Ref.4, and Refs. 2 and 3 has been a subject of some controversy, most clearly stated in Ref. 3. It has been argued already by the present authors and Carbotte that the experimental results from these groups are in fact in agreement,[62] and here we elaborate further on the sources of the apparent differences. We interpret $\delta C(T,H)$ as a pure vortex quantity, ignoring the possible elastic contribution of the vortex lattice and the possible field dependence of the anisotropy $\eta = E_{ab}/E_H$. The issues raised in Ref. 3 include the temperature dependence of $\delta C(T,H)/T$ in the regime where $C(T,H)/T$ is essentially insensitive to temperature, and a form of the scaling function for $\delta C$ that is quite different from that of $C(T,H)$.

As is clear from Fig. 8 for the field $\mathbf{H} \| \hat{\mathbf{c}}$ the ratio $C(T,H)/T$ does not depend strongly on the temperature for $T \lesssim T_H \sim (0.1-0.25)E_H$, reflecting the energy independence of the density of states for $\omega \ll E_H$. For the field applied in the plane along the antinodal direction the physics is very similar, up to rescaling of the energies, which means that the density of states is only constant for $\omega \ll E_{ab} \ll E_H$, and therefore $C(T,H;0)/T$ is $T$ dependent above $T_{ab} \sim (0.1-0.25)E_{ab}$. The difference, $\delta C/T$, becomes temperature dependent at the lower of the two crossovers, which is at $T \simeq 0.1E_{ab}$, and for $T_{ab} \lesssim T \lesssim T_H$ it varies with temperature even though $C(T,H)/T$ is approximately constant.

It is easy to understand the difference in the scaling behavior between $\delta C$ and $C(T,H)$. Taking the ratio $E_H/E_{ab} = 4$ we plot the corresponding scaling functions in Fig. 9. Even in the regime where the scaling function $F_C$ is nearly constant $F_{\delta C}$ is decreasing continuously. We therefore believe that there is no contradiction between the results of Ref. 5, and Refs. 2 and 3. Both the temperature dependence of $\delta C/T$ and the difference in the behavior of the scaling function reflect the smaller Doppler energy scale in the plane, $E_{ab} \ll E_H$, and the results of these experiments are, in fact, quite consistent. Notice that the crossover in $\delta C$ is much wider than that in $C(T,H)$ because of two energy scales contributing to it: it extends over a decade in the scaling variable. Note that in Fig. 9 we have evaluated the specific heat with the field $\mathbf{H} \| \hat{c}$ in the single-vortex approximation, while the specific heat for the field along the antinode in the plane has been evaluated for the liquid I distribution, to model the expected difference in the degree of order in the vortex lattice. Both quantities have been evaluated with the single-vortex distribution in a prior publication,[62] and there are no qualitative differences between the two cases.

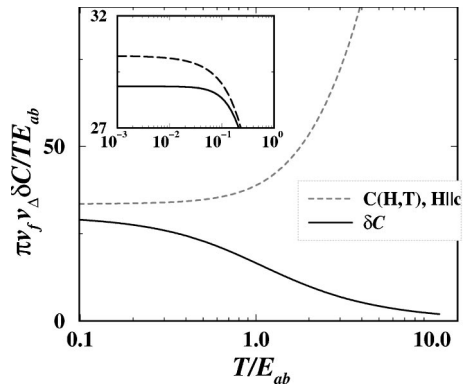


FIG. 9. Scaling functions for the specific heat with the field applied along the *c* axis, $C(T,H)$ and the $c/a-b$ difference $\delta C = C(T,H) - C(T,H;0)$. The former has been evaluated for the single-vortex distribution of the Doppler shift, the latter for the liquid I model as explained in the text. The behavior remains essentially unmodified for other forms of the distribution. Inset: difference between the nodal (top) and antinodal directions disappears on the scale of the larger graph.

To further quantify these considerations we note that even though the crossover to the temperature insensitive $\delta C$ has not been found in Ref. 4, the data suggest that it is close to $T/\sqrt{H} \sim 0.5$ K T$^{-1/2}$, which is the lowest value of the scaling variable reached in the paper (experimental measurements are limited to the temperatures above $\sim 1.5$ K, since at lower temperatures the nonvortex contributions to $C(T,H)$ become dominant). Taking this number as a crossover value of $T/E_{ab}$, we estimate $E_{ab}/\sqrt{H} \sim 3-4.5$ K T$^{-1/2}$; 2–3 times smaller than the estimate from the London model.

If the value of $E_{ab}$ is low, it is not surprising that the in-plane anisotropy between the nodal and the antinodal directions has not been found in the experiments of Ref. 5: at 14 T, $E_{ab} \approx 11-17$ K, and even at the lowest temperature where the measurements of Ref. 5 have been made $T/E_{ab} \gtrsim 0.09-0.15$. Then the anisotropy in the density of states is significantly reduced from the $T=0$ value, see the inset of Fig. 9. On the other hand, the data of Ref. 5 for the field in the plane yield (after the subtraction of the Schottky anomaly) a crossover temperature between the field-dominated and the temperature-dominated regimes close to $T_{cr} \approx 2$ K T$^{1/2}$. If this value is taken as corresponding to the

crossover in $T/E_{ab}$, it implies a large value of $E_{ab}/\sqrt{H} \geqslant 10-20$ K T$^{-1/2}$. In that case the absence of the anisotropy can only be explained (somewhat unsatisfactorily) by an appeal to the three-dimensionality[17] or a combination of the orthorhombicity and twinning.[17,60] Since part of the experimental difficulty stems from the smallness of the $\sqrt{H}$ term with the field in the plane, the analysis for that geometry typically involves assuming a field-dependent contribution of that form.[2,5] However, if $E_{ab}$ is small, the field dependence of the specific heat is modified by the Zeeman splitting, and this splitting has to be taken into account in the analysis.

### C. Zeeman splitting

If the energy scale for the in-plane Doppler shift is indeed much smaller than the naive estimate from the London model, $E_{ab}/\sqrt{H} \sim (3-4.5)$ K T$^{-1/2}$, the Zeeman splitting has a significant effect on the specific heat with the field applied along a node in the experimentally relevant range. The specific heat no longer obeys the scaling properties discussed above; for the field along a node the contribution of the Doppler-''inactive'' nodes is given by

$$C_Z(T,H) = \frac{T^2}{\pi v_f v_\Delta} F_Z\left(\frac{\mu H}{T}\right) \tag{73}$$

$$F_Z(x) = x\int_0^x t^2 \cosh^{-2}\frac{t}{2}\,dt + \int_x^\infty t^3 \cosh^{-2}\frac{t}{2}\,dt, \tag{74}$$

in agreement with Ref. 64, and therefore scales with $H$ rather than $\sqrt{H}$.

As the in-plane anisotropy in the density of states has a maximum for $\omega = \mu H$, the anisotropy in the specific heat also goes through a maximum; we expect approximately $T_{max}(H) \propto H$. We consider here two different cases for $a = E_{ab}/\sqrt{H}$: a large value corresponding to our original estimate $a = 10$ K T$^{-1/2}$, and a small value implied by the experiment, $a = 4$ K T$^{-1/2}$, and evaluate the specific heat for the liquid I distribution. The main panel of Fig. 10 shows the scaling plot for the in-plane anisotropy in the specific heat, $C_{anis}(T,H) = C(T,H;0) - C(T,H;\pi/4)$ at $H = 10$ T, so that the values for the two cases are $E_{ab} \simeq 32$ K, and $E_{ab} \simeq 13$ K. While the anisotropy is severely reduced at $T = 0$, it becomes close to the values estimated without accounting for the Zeeman shift at the temperatures $T \simeq 2.2$ K and $T \simeq 1.8$ K for the two cases, respectively, and therefore the anisotropy in the experimentally relevant regime is not modified significantly. Nevertheless, if the absolute magnitude of the anisotropic term is small, and its field dependence has to be modeled in the analysis of the experimental results,[5] it is important to note that, as is clear from the inset of Fig. 10, the field dependence of the anisotropy is not simply proportional to $\sqrt{H}$, but flattens and decreases at high fields. The deviations are especially important for small $a$, since then the maximum of the anisotropy is reached at $H \sim 10$ T for $T = 1.5$ K, well within the experimental range. We analyze this scenario in more detail in Fig. 11, which demonstrates that if the coefficient $a$ is small, the maximum in the anisotropy can be observed at low temperatures, but moves out of the easily accessible range, to $H \geqslant 20$ T, at higher $T$. In comparison, if $a \sim 10$, the maximum lies at high fields for all relevant $T$. Consequently, in the search for the experimental verification of the anisotropy in the specific heat, it cannot be assumed that the anisotropy increases as $\sqrt{H}$; if the energy scale for the in-plane Doppler shift is small, the Zeeman splitting modifies the field dependence of the specific heat. For the small value $a = 4$ K T$^{-1/2}$ the maximum anisotropy, reached in the fields of the order of 10–15 T at $T = 1.5-3$ K, is of the order of $0.5-0.9\gamma_s$; based on the available experimental values[2,3,5] for $\gamma_s$ between 0.064 and 0.21 (mJ mol$^{-1}$) K$^{-3}$, the maximal anisotropy ranges between 0.032 and 0.19 mJ mol$^{-1}$ K$^{-1}$; it is significantly larger for larger values of $E_{ab}/\sqrt{H}$.

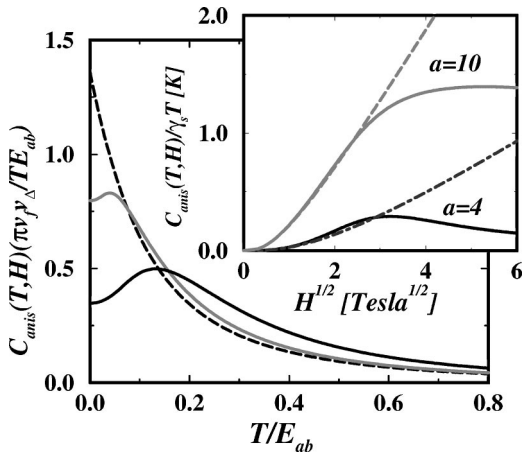


FIG. 10. Main panel: the anisotropy in the in-plane specific heat plotted in the scaling form at $H = 10$ T for the coefficient $a = (4,10)$ K T$^{-1/2}$, and without accounting for the Zeeman shift (dashed line). Inset: The specific heat at $T = 1.5$ K, which is close to the lowest experimentally accessible temperature, for the same two values of $a$ with (solid line) and without (dashed line) accounting for the Zeeman shift.

Recently, Wang *et al.* attempted to observe the angular oscillations we have predicted in the in-plane specific heat.[5] They did not, however, find appreciable difference between two measurements with field applied in the nodal and antin-

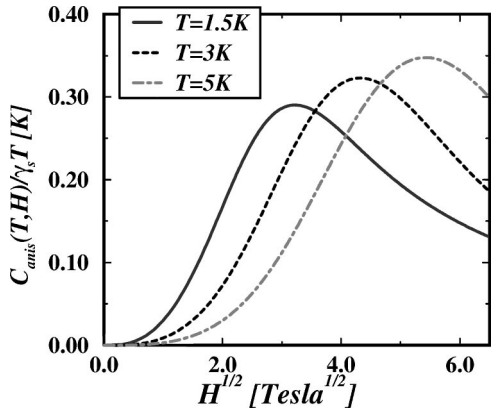


FIG. 11. Anisotropy of the in-plane specific heat for $a = 4$ K T$^{-1/2}$ as a function of the field at different temperatures.

odal directions. Several reasons may have contributed: first of all, the YBCO sample used in their experiment is twinned. Twinning, combined with the orthorhombicity of YBCO is expected to reduce the anisotropy.[17,60] Here we point out another possible reason for the difficulty in extracting the difference between the two directions from the data: the field dependence of the anisotropic term is not simply given by $\sqrt{H}$, as it would be in the absence of the Zeeman term, and as assumed in Ref. 5. Instead, the anisotropy increases with the field up to fields of about 10–15 T, and decreases thereafter. Consequently, we believe that to confirm the predicted oscillations experimentally, it is highly desirable to use an untwinned crystal, and carry out the measurements at intermediate fields (10–15 T) at the lowest possible temperatures, since the anisotropy in the specific heat is expected to be the largest in this range.

## VII. SPIN-LATTICE RELAXATION RATE

We now turn our attention to the calculation of the response functions. In these calculations the local, in real space, physical quantities depend on the Doppler shift at both pairs of nodes, and consequently the averaging has to be carried out with the two-node probability density $\mathcal{L}$ rather than the single-node distribution $\mathcal{P}$. The simplest example of such a quantity is the average spin-lattice relaxation rate that we now consider.

Since the NMR measurements on cuprates are typically done in a magnetic field of $\sim 10$ T, the effect of the field on the measured signal has to be considered in the analysis of the data. There are at least two effects of the vortex state on the spin-lattice relaxation time. First, the Doppler shift modifies the local density of states, introducing the local relaxation rate, which varies from point to point. Second, the magnetization due to the vortex lattice introduces inhomogeneities in the field, leading to the broadening of the resonance line. As a result, there are two possible approaches to the analysis. In a perfect vortex lattice there exists a one-to-one correspondence between the local field at a particular point in the unit cell of the vortex lattice, and the value of the superfluid velocity at that point. Assuming such a perfect lattice it is therefore possible to associate the local relaxation rate with the relaxation rate at a particular frequency in the resonant line. Such an approach has been developed theoretically in the semiclassical framework,[55,66] and the results are in qualitative agreement with the experimental observation that the relaxation rate and the local density of states are larger in the regions of higher field, i.e., higher supervelocity.[8]

On the other hand, in a disordered vortex state there is no unique identification of the local value of the supervelocity corresponding to a local magnetic field. It may therefore be useful to analyze the relaxation rate obtained by the ''global'' fit to the resonance line; especially when the linewidth remains quite narrow in frequency. It has been shown that the time-decay of the magnetization is nonexponential as it involves a convolution of many local relaxation rates, but that it is possible to describe it with an effective scattering rate that depends on the field and the temperature.[16,67] Usually the analysis of the experimental data is done assuming a single relaxation rate, and it is therefore important to understand its behavior in a *d*-wave superconductor.

The analysis of the relaxation time $T_1$ can be undertaken either by looking at its magnitude directly, or by analyzing the ratio $T_1/\tau_c$, where $\tau_c$ is the relaxation time at $T=T_c$. The former approach involves modeling or estimating from the available data the matrix element for the interaction; it has been used, for example, in Ref. 55. The latter method is based on making assumptions about the normal state relaxation in the cuprates. We employ it assuming a normal metallic relaxation at $T_c$ with the caveat that this may be only qualitatively correct for underdoped compounds.

With this assumption for the spin-$\frac{1}{2}$ system the magnetization decays as $m(t)=M(t)/M(0)=\exp(-t/T_1)$, where the relaxation rate in the infinitesimal field is given by

$$\frac{\tau_c T_c}{T_1 T}=\int_{-\infty}^{+\infty} d\omega \frac{N^2(\omega)}{N_0^2}\left(-\frac{\partial f}{\partial \omega}\right)$$

$$=\frac{1}{2}\int_0^{+\infty} dx \frac{N^2(xT)}{N_0^2}\cosh^{-2} x/2, \tag{75}$$

where $N_0=m/2\pi\hbar^2$ is the two-dimensional (2D) density of states in the normal state.

In nonzero magnetic field, the decay of the average magnetization is given by

$$m(t)=4\int_0^{\infty} d\epsilon_1 \int_0^{\infty} d\epsilon_2 \mathcal{L}(\epsilon_1,\epsilon_2)\exp[-t/T_1(\epsilon_1,\epsilon_2)], \tag{76}$$

where the position and Doppler-shift-dependent relaxation rate is determined from

$$\frac{\tau_c T_c}{T_1 T}=\frac{1}{2N_0^2}\int_0^{+\infty} dx N^2(xT,\epsilon_1,\epsilon_2)\cosh^{-2} x/2. \tag{77}$$

The density of states is given by the sum of the contributions of all nodes, $|\omega+\epsilon_i|/(\pi v_f v_\Delta)$ with $(\epsilon_i=\pm\epsilon_1,\pm\epsilon_2)$, which yields

$$N(\omega,\epsilon_1,\epsilon_2)=\frac{1}{2\pi v_f v_\Delta}\begin{cases} 2\omega, & \text{if } \omega \geqslant \max(\epsilon_1,\epsilon_2); \\ \omega+\max(\epsilon_1,\epsilon_2), & \text{if } \min(\epsilon_1,\epsilon_2)\leqslant\omega\leqslant\max(\epsilon_1,\epsilon_2); \\ \epsilon_2+\epsilon_1, & \text{if } \omega\leqslant\min(\epsilon_1,\epsilon_2). \end{cases} \tag{78}$$

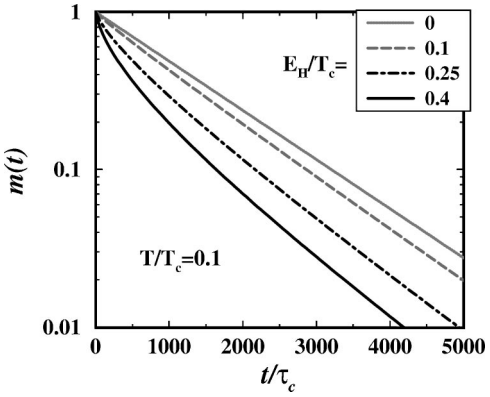


FIG. 12. Magnetization decay at a fixed temperature for different values of the magnetic field. We have used $2N_0\pi v_f v_\Delta = k_f v_\Delta \approx 2\Delta_0$ (pure $d$ wave), and have set $\Delta_0 = 2.14T_c$. $m(t)$ has been evaluated for the liquid I model.

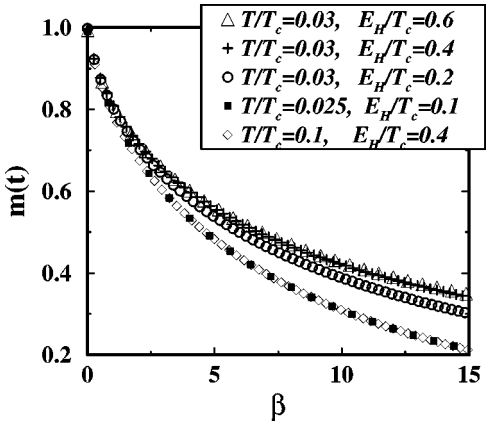


FIG. 13. Magnetization as a function of $\beta = tTE_H^2/\tau_c T_c \Delta_0^2$. The ratio $T/E_H$ is identical for the bottom two sets.

Here again, without loss of generality, we set $\omega, \epsilon_1, \epsilon_2 \geqslant 0$.

The decay of the magnetization is therefore nonexponential,[16,67] as is shown in Fig. 12 for a liquid distribution. In a magnetic field the density of states is enhanced globally, and therefore the stronger the field the faster the decay of $m(t)$. In the regime $E_H \gg T$ the density of states is significantly enhanced over a large part of the unit cell of the vortex lattice. This high density of states yields a fast relaxation rate responsible for the initial decrease in the magnetization. The long-time decay of $m(t)$ is determined by the slowest relaxation rates, which occur in the regions where the superfluid velocity is small and the density of states is largely determined by the temperature. The two regimes are seen in Fig. 12: the large-$t$ tail of $\ln m(t)$ is affected by the field much more weakly than the short-time decay. For all the values of the field it is possible to fit the time dependence by an exponential, although clearly the relaxation rate obtained from such a fit differs significantly from the zero-field rate. We have addressed the fit of the magnetization at different time scales in a previous publication.[16,67]

An important comment concerns the scaling of the magnetization. First of all, due to scaling properties of the density of states, the magnetization decay due to spin-lattice relaxation satisfies

$$m(t) = F_m\left( tHTf\left( \frac{T}{\sqrt{H}} \right) \right), \tag{79}$$

where the functions $F_m$ and $f$ can be obtained from the general expression Eq. (76). Moreover, when $E_H/T \gg 1$ the density of states and therefore the function $f$ are nearly constant. Two conclusions follow immediately. First, at a fixed ratio $T/\sqrt{H}$ the magnetization depends only on the single variable $tTH$. Second, at low temperatures $m(tTH)$ is independent of the ratio $T/\sqrt{H}$ at short time scales, when the relaxation rate is dominated by the field-induced density of states rather than the temperature-driven density of states. The collapse of the low-$T$ data on a single curve as a function of $tT$ has been found previously;[9,68] however, we are not aware of an experimental check of such scaling at different fields. In Fig. 13 this behavior is clearly seen. Deviations from the scaling form are noticeable already for $E_H/T \sim 4$; however, even in this regime the curves for different $E_H$ and $T$ but with the same ratio $E_H/T$, coincide. The scaling is always obeyed at short time scales, where the time decay of the magnetization is determined by the fast relaxation rates in the regions with a large Doppler shift. On the other hand, at long time scales the time-dependence of $m(t)$ is determined by the slowest relaxation rates, in the regions where the Doppler shift vanishes, and therefore there are always deviations from the scaling with $tTH$.

Since the long-time-scale decay is determined by the measure of the points with small Doppler shift, it depends crucially on the probability density $\mathcal{L}(\epsilon_1, \epsilon_2)$. In particular, there is a dramatic difference between the single-vortex picture, where $\epsilon_1^2 + \epsilon_2^2 \geqslant E_H^2$, and the lattice or liquid states, where this restriction is lifted: magnetization decays much faster in the single-vortex picture, as can be seen in Fig. 14. Notice that for the very early times, when the magnetization decay is determined by the regions with the highest Doppler shift, the two distributions give the same result. Therefore the effective relaxation rate obtained from the exponential fit depends not only on the field but also on the structure of the vortex state. The difference in the behavior for the two types of the vortex state can be understood from the analysis of the

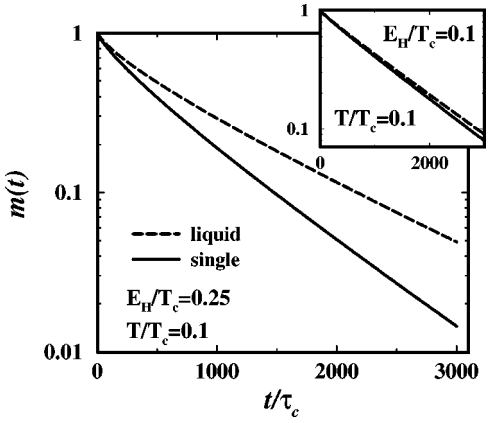


FIG. 14. The difference between the liquid (liquid I) and the single-vortex models in a strong (main panel) and weak (inset) magnetic field. Parameters are the same as in Fig. 12.

magnetization. Noticing that $\mathcal{L}(\epsilon_1,\epsilon_2)=\mathcal{L}_1(\epsilon_1^2+\epsilon_2^2)$ due to symmetry (the probability density should be even in both $\epsilon_1$ and $\epsilon_2$, and should be symmetric under the interchange $\epsilon_1 \leftrightarrow \epsilon_2$), and introducing polar coordinates $x=(\epsilon_1^2+\epsilon_2^2)/E_H^2$, $\tan\phi=\epsilon_1/\epsilon_2$, we arrive at

$$m(t)\approx \int_{x_0}^{\infty} dx \mathcal{L}_1(x) e^{-\beta x/4} I(\beta x/4), \tag{80}$$

$$I(z)=\int_0^{\pi} \exp(-z\sin\phi) d\phi, \tag{81}$$

where $x_0 \approx T^2/E_H^2$, and $\beta = tTE_H^2/\tau_c T_c \Delta_0^2$. This form shows explicitly that there is an approximate scaling with the variable $\beta$, and that the scaling is obeyed better the smaller the ratio $T/E_H$.

Due to the exponential the integral over $x$ is cut off at $\beta x \gg 1$, so that we only need to evaluate $I(z)$ for $z\sim 1$. In that case all angles $\phi$ contribute to the integral, and $I(z) \approx \pi \exp(-bz)$ with $b\sim 1$ [in contrast, $I(z)\simeq 2/z$ for $z\gg 1$], leading to

$$m(t)\approx \pi \int_{x_0}^{\infty} dx \mathcal{L}_1(x) e^{-\beta s x/4}, \tag{82}$$

with $s=1+a\sim 1$. Consequently, the long-time-scale limits ($\beta \gg 1$) for the single-vortex and liquid I distribution, respectively

$$m(t)=\int_1^{\infty} dx \frac{e^{-\beta s x/4}}{x^2} \sim \frac{\exp(-\beta s/4)}{s\beta/4}, \tag{83}$$

$$m(t)=\int_{x_0}^{\infty} dx \frac{e^{-\beta s x/4}}{(x+1)^2} \sim \frac{\exp(-\beta s x_0/4)}{s\beta/4}. \tag{84}$$

As a result, the long time decay for the liquid regime is governed by the relaxation rate close to the $\beta x_0 \propto T^3$ behavior expected for $H=0$, while for the single-vortex model the relaxation rate is proportional to $\beta \propto TH$.

In reality, however, the decay of $m(t)$ at long time scales is usually not measured, and at intermediate times the detailed analysis of the time dependence of the magnetization taking into account the nonexponential form of $m(t)$ is complex. It is possible to define an effective relaxation rate, however, the weight of the components of the magnetization with fast and slow decay is different for different definitions, and the resulting effective relaxation rate is different, as we now illustrate. One possible approach is to define the effective *rate* as

$$\frac{1}{T_1^{eff}}=4\int_0^{\infty} d\epsilon_1 \int_0^{\infty} d\epsilon_2 \mathcal{L}(\epsilon_1,\epsilon_2) \frac{1}{T_1(\epsilon_1,\epsilon_2)}. \tag{85}$$

Unlike the average for the magnetization, Eq. (76), which has the largest contribution from the slowest relaxation rates, in this averaging procedure the weight of short relaxation rates is high, and a cutoff of the energy integral near the core is required. To leading order in $\ln E_0/E_H$ the relaxation rate in the field-dominated regime is then given by

$$\frac{1}{T_1^{eff}} \approx \frac{\pi+2}{2\pi} \frac{1}{\tau_c} \frac{T}{T_c} \frac{E_H^2}{\Delta_0^2} \ln \frac{E_0}{E_H}. \tag{86}$$

The relaxation rate given by this expression is expected to overestimate the rate of the decay of the magnetization. Fast relaxation occurs near the cores, where the effective field is higher, and therefore in the component of the signal away from the original position of the resonance line.[55] Alternatively, we can define the average relaxation *time*

$$\tau_1^{eff}=\int_0^{\infty} m(t) dt = 4\int_0^{\infty} d\epsilon_1 \int_0^{\infty} d\epsilon_2 \mathcal{L}(\epsilon_1,\epsilon_2) T_1(\epsilon_1,\epsilon_2). \tag{87}$$

This average has a large contribution from slow relaxation rates, and we expect the effective rate to be underestimates since over experimentally relevant time scales the slowest rates do not contribute to the magnetization decay appreciably. Indeed, for the cases of the single-vortex and the liquid distributions we obtain in the field-dominated regime

$$\frac{1}{\tau_1^{eff}} \approx \frac{\pi}{8} \frac{1}{\tau_c} \frac{T}{T_c} \frac{E_H^2}{\Delta_0^2}, \quad \text{single vortex,} \tag{88}$$

$$\frac{1}{\tau_1^{eff}} \approx \frac{\pi}{32} \frac{1}{\tau_c} \frac{T}{T_c} \frac{E_H^2}{\Delta_0^2} \left[\ln \frac{E_H}{T}\right]^{-1}, \quad \text{liquid I.} \tag{89}$$

The coefficient in the last expression is significantly smaller than the expression given by Eq. (86). We can now compare this expression with the result of Ref. 9, where it was found that $\tau_c T_c/T_1 T \approx 0.2$ at $H=11$ T at low $T$. From our estimate of $E_H$ it follows that at this field $E_H \sim 100$ K. Taking $E_0 \simeq 1500$ K, we find this ratio for the average rate to be 0.35, while the average relaxation time procedure yields the values of 0.06 and 0.005 (at $T\simeq 5$ K), respectively. The experimental value is between the two estimates, as expected.

## VIII. IMPURITY SCATTERING

### The self-energy

In the presence of impurity scattering the frequency is renormalized according to $\tilde{\omega}=\omega-\Sigma(\tilde{\omega})$. The self-energy $\Sigma(\tilde{\omega})$ depends on the momentum integral of the Green's function, and therefore on the Doppler shifts at all nodes. Consequently, in all the calculations involving the impurities, the local quantities depend on both $\epsilon_1$ and $\epsilon_2$.

Here we consider the impurity scattering in the unitarity limit. The strategy for the calculation is as follows. The self-energy is given by Eq. (6); to evaluate this expression in a field we have to introduce the Doppler shift in the Green's function as before, and solve for the self-energy self-consistently at each node. In other words, there is a distinct Doppler shift at each node, and the self-consistency requires that the scattering to other nodes with their respective Doppler shifts be taken into account self-consistently. Therefore we can write

$$\Sigma(\tilde{\omega},\epsilon_1,\epsilon_2)=-n_i[G_0(\tilde{\omega},\epsilon_1,\epsilon_2)]^{-1}, \tag{90}$$

where, from Eq. (8),

$$G_0(\tilde{\omega},\epsilon_1,\epsilon_2) = -\frac{1}{2\pi}\sum_{\substack{\alpha=\pm\\ n=1,2}}\frac{\omega_{\alpha,n}+i\omega_2}{v_f v_\Delta} \times\left[\ln\frac{E_0}{\sqrt{\omega_{\alpha,n}^2+\omega_2^2}}+i\arctan\frac{\omega_{\alpha,n}}{\omega_2}\right], \quad (91)$$

and

$$\omega_{\alpha,n} = \omega+\alpha\epsilon_n-\mathrm{Re}\,\Sigma(\tilde{\omega},\epsilon_1,\epsilon_2), \quad (92)$$

$$\omega_2 = -\mathrm{Im}\,\Sigma(\tilde{\omega},\epsilon_1,\epsilon_2). \quad (93)$$

We now focus our attention on the cases of weak $\omega \ll E_H \ll \gamma$, and strong $\omega \ll \gamma \ll E_H$ fields at low temperatures. Setting $\omega=0$ it is clear immediately that the real part of the momentum integral of the Green's function at each node in Eq. (91) is odd in the Doppler shift, $\epsilon_n$, and therefore vanishes upon summation.[14] As a result, the self-energy has only the imaginary part given by Eq. (90) with

$$G_0(\tilde{\omega},\epsilon_1,\epsilon_2) = -\frac{i}{\pi}\frac{\omega_2}{v_f v_\Delta}\ln\frac{E_0^2}{\sqrt{\epsilon_1^2+\omega_2^2}\sqrt{\epsilon_2^2+\omega_2^2}} -\frac{i}{\pi}\frac{\epsilon_1}{v_f v_\Delta}\arctan\frac{\epsilon_1}{\omega_2}-\frac{i}{\pi}\frac{\epsilon_2}{v_f v_\Delta}\arctan\frac{\epsilon_2}{\omega_2}. \quad (94)$$

In the strong-field limit, $\omega_2 \ll \epsilon_1,\epsilon_2$, we obtain for the the density of states

$$N(\epsilon_1,\epsilon_2) = -\frac{1}{\pi}\mathrm{Im}\,G_0(\tilde{\omega},\epsilon_1,\epsilon_2) = \frac{1}{2\pi}\frac{|\epsilon_1|+|\epsilon_2|}{v_f v_\Delta}, \quad (95)$$

as expected, see Eq. (78). The quasiparticle damping in this regime is given by

$$\omega_2 \approx \frac{2n_i v_f v_\Delta}{|\epsilon_1|+|\epsilon_2|} \sim \frac{\gamma^2}{|\epsilon_1|+|\epsilon_2|} \ll \gamma. \quad (96)$$

In the weak-field impurity-dominated regime, $\omega_2 \gg \epsilon_1,\epsilon_2$, on the other hand, the field-induced change in the density of states is quadratic in the Doppler shift and is given by

$$\delta N(\epsilon_1,\epsilon_2) \approx \frac{1}{4\pi^2 v_f v_\Delta}\frac{\epsilon_1^2+\epsilon_2^2}{\gamma}, \quad (97)$$

where $\gamma$ is the zero energy-scattering rate that has been defined in Sec. III. Then to the leading order in $\ln E_0/E_H$ the average change in the density of states is given by

$$\delta N_s(0,H) \approx \frac{E_H^2}{2\pi^2\gamma v_f v_\Delta}\ln\frac{E_0}{E_H} \propto H\ln\frac{H_0}{H} \quad (98)$$

for the single-vortex and the liquid distributions. For the Gaussian model the change in the density of states is smaller by a logarithm of a large number, $\delta N_s(0,H)/\delta N_G(0,H) = 2\ln E_0/E_H$. This behavior is illustrated in Fig. 15. Notice that the three distributions yield different high-field slopes, corresponding to the different values of the moment $M_1$. These results are in agreement with the previous work.[14,18] The low energy-scattering rate, $\gamma$, provides the new energy scale in addition to the average Doppler shift $E_H$ and the temperature $T$. At low temperatures, the competition between $E_H$ and $\gamma$ determines the behavior of the density of states, and in the field-dominated regime, $E_H \gg \gamma$, the density of states strongly depends on the probability density of the Doppler shift, as it does in the pure limit. The dependence of the self-energy on the magnetic field is crucially important for the analysis of the transport properties in the vortex state, and we will discuss these issues in detail in a separate paper.

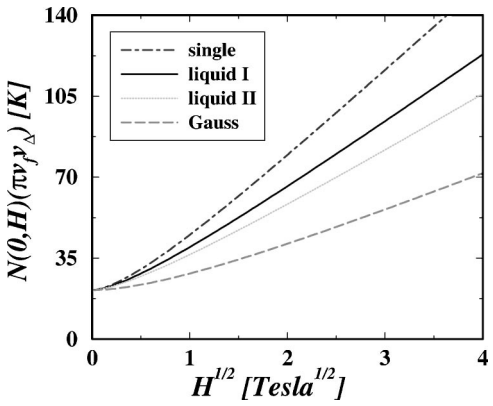


FIG. 15. Residual density of states as a function of the field. The impurity scattering is taken in the unitarity limit, with $(n_i\pi v_f v_\Delta)^{1/2}=20$ K. The parameters are $E_0=1500$ K, $E_H/\sqrt{H}=30$ K $\mathrm{T}^{-1/2}$.

## IX. CONCLUSIONS

In this paper we have discussed the semiclassical approach to the vortex state of unconventional superconductors and have applied it to the analysis of the thermodynamic properties of a two-dimensional *d*-wave superconductor, which we take as a model for the high-$T_c$ cuprates at low energies. Our main point is that within the semiclassical approach the dependence of the measured quantities on the magnetic field is sensitive to the structure of the vortex state and the distribution of the supercurrents. This is shown in an approach that involves introducing the Doppler shift due to circulating supercurrents into the quasiparticle dispersion, and computing the physically measured magnetic field dependent quantities as a spatial average of their local values in the vortex state. The major step that has enabled us to move beyond the standard single-vortex description is the rewriting of the spatial average in terms of the average over a probability density of the Doppler shift at a particular node or at a pair of nodes. We have analytically computed these probability densities for the single-vortex picture, for model liquid distributions, and for a nonphysical, albeit often used, completely random distribution. We have argued that this approach is easily applicable to any given distribution of vortices, and that the single-vortex and the liquid models typically give the upper and the lower limits of the field dependence since they overestimate and underestimate, re-

spectively, the number of the points in the vortex lattice unit cell where the Doppler shift dominates the physical picture.

We have applied this approach to the analysis of the electronic specific heat in the vortex state and to the description of the spin-lattice relaxation of the NMR magnetization. In the former case the specific heat depends on the single-node probability distribution. The values for the Fermi velocity at the nodes, as well as of the slope of the superconducting gap, determined from such an analysis are consistent with the values inferred from other experimental measurements, and the values directly determined from the photoemission. Moreover, noticing that the magnitude of the $\sqrt{H}$ term is larger for the more ordered vortex state, has allowed us to reduce the discrepancy between the results for the gap slope obtained by different experimental groups. We have also emphasized that the difference in the form of the scaling function obtained by these groups is naturally explained as a consequence of the smaller Doppler shift energy scale for the field applied in the plane; this work confirms our earlier assessment on the basis of the single-vortex picture.[62]

Since the analysis of the scaling plots allowed us to estimate the energy scale of the Doppler shift for the field in the plane, and since this energy scale is smaller than the London model estimate of our previous work,[17] we have investigated here whether the anisotropy in the specific heat between the experimental arrangements with the field applied along a node and between the two nodes is observable. We have paid special attention to the effect of the Zeeman splitting, which becomes more important for smaller in-plane scale $E_{ab}$. We have found that, while the zero-temperature anisotropy is significantly reduced compared to the case of no Zeeman splitting, as predicted,[20] the anisotropy does not decrease with the temperature and in the experimentally relevant temperature range the magnitude of the anisotropy is weakly affected by the inclusion of the Zeeman splitting. The field dependence of the anisotropic specific heat may, however, be modified quite significantly, and this change has to be taken into account when analyzing the experimental data.

We have considered the spin-lattice relaxation rate as an example of a response function that depends on the probability distribution at two nodes; in contrast to the specific heat the contributions of the nodes are not simply additive. It has been known that the magnetization decay is nonexponential due to a distribution of the local relaxation times.[16] We have shown here that the effective relaxation rate obtained from a fit to an exponential at short or long time scales is different, and at long times depends crucially on the structure of the vortex state. We have predicted a scaling form of the magnetization, and discussed the existing evidence for such a scaling; of course more experimental work checking this prediction would be highly desirable. We have also introduced an effective relaxation rate obtained from a global fit to the magnetization, and found that it agrees qualitatively with the available experimental results.

In general, the structure of the vortex state may change quite dramatically as the temperature and the applied field are varied; one example of such a change is the melting of the vortex lattice. In such a situation we expect a change in the spatially averaged thermodynamic quantities measured in experiment that reflects the transition from one type of distribution to another. Moreover, as the degree of ordering in the vortex lattice depends on the history of the sample, the measured field dependence varies accordingly. For example, the coefficient of the $\sqrt{H}$ term in the electronic specific heat should, in general, depend on whether the sample has been cooled in an applied field or in zero field: in the latter case the vortex state is more disordered. Whether these effects are observable experimentally depends crucially on the quality of the sample since the changes may be rather small, nevertheless, in clean, untwinned samples they may be measurable.

Finally, to illustrate that in the presence of impurities the two-node probability density is always required we have analyzed the density of states in the impurity-dominated regime for different structures of the vortex state. This part of our work will be developed further in the analysis of the transport properties, which warrants a separate paper.

## ACKNOWLEDGMENTS

It is a pleasure to acknowledge discussions and correspondence with L. N. Bulaevskii and A. E. Koshelev. This research has been supported in part by the Department of Energy under Contract No. W-7405-ENG-36 (I.V.), by the NSF through Grant No. DMR-9974396 (P.J.H.), and by NSERC of Canada, Cottrell Scholar program of Research Corporation, and the Premier's Research Excellence Award of the Government of Ontario, Canada (E.J.N.). I.V. acknowledges Aspen Center for Physics for hospitality during the early stages of this work. I.V. and P.J.H. are grateful for hospitality and support of ITP Santa Barbara via Grant No. NSF-PHY-94-07194.

*Email address: vekhter@viking.lanl.gov

[1] D. J. Van Harlingen, Rev. Mod. Phys. **67**, 515 (1995).

[2] K. A. Moler, D. J. Baar, J. S. Urbach, R. Liang, W. N. Hardy, and A. Kapitulnik, Phys. Rev. Lett. **73**, 2744 (1994); K. A. Moler, D. S. Sisson, J. S. Urbach, M. R. Beasley, A. Kapitulnik, D. J. Baar, R. Liang, and W. N. Hardy, Phys. Rev. B **55**, 3954 (1997).

[3] D. A. Wright, J. P. Emerson, B. F. Woodfield, J. E. Gordon, R. A. Fisher, and N. E. Phillips, Phys. Rev. Lett. **82**, 1550 (1999).

[4] B. Revaz, J.-Y. Genoud, A. Junod, K. Neumaier, A. Erb, and E. Walker, Phys. Rev. Lett. **80**, 3364 (1998).

[5] Y. Wang, B. Revaz, A. Erb, and A. Junod, Phys. Rev. B **63**, 094508 (2001); A. Junod, B. Revaz, Y. Wang, and A. Erb, Physica B **284-288**, 1043 (2000).

[6] S. J. Chen, C. F. Chang, H. L. Tsay, H. D. Yang, and J.-Y. Lin, Phys. Rev. B **58**, R14 753 (1998); C. F. Chang, J.-Y. Lin, and H. D. Yang, *ibid.* **61**, 14 350 (2000).

[7] J. E. Sonier, J. H. Brewer, R. F. Kiefl, G. D. Morris, R. I. Miller, D. A. Bonn, J. Chakhalian, R. H. Heffner, W. N. Hardy, and R. Liang, Phys. Rev. Lett. **83**, 4156 (1999); J. E. Sonier, R. F. Kiefl, J. H. Brewer, D. A. Bonn, S. R. Dunsinger, W. N. Hardy, R. Liang, W. A. MacFarlane, T. M. Riseman, D. R. Noakes, and C. E. Stronach, Phys. Rev. B **55**, 11 789 (1997); J. E. Sonier, J. H.

Brewer, R. F. Kiefl, D. A. Bonn, S. R. Dunsinger, W. N. Hardy, R. Liang, W. A. MacFarlane, R. I. Miller, T. M. Riseman, D. R. Noakes, C. E. Stronach, and M. F. White, Jr., Phys. Rev. Lett. **79**, 2875 (1997).
[8] N. J. Curro, C. Milling, J. Haase, and C. P. Slichter, Phys. Rev. B **62**, 3473 (2000).
[9] G.-q. Zheng, W. G. Clark, Y. Kitaoka, K. Asayama, Y. Kodama, P. Kuhns, and W. G. Moulton, Phys. Rev. B **60**, R9947 (1999).
[10] M. Chiao, R. W. Hill, C. Lupien, B. Popić, R. Gagnon, and L. Taillefer, Phys. Rev. Lett. **82**, 2943 (1999).
[11] H. Aubin, K. Behnia, S. Ooi, and T. Tamegai, Phys. Rev. Lett. **82**, 624 (1999).
[12] K. Krishana, N. P. Ong, Q. Li, G. D. Gu, and N. Koshizuka, Science **277**, 83 (1997).
[13] G. E. Volovik, Pis'ma Zh. Eksp. Teor. Fiz. **58**, 457 (1993) [JETP Lett. **58**, 469 (1993)].
[14] C. Kübert and P. J. Hirschfeld, Solid State Commun. **105**, 459 (1998).
[15] C. Kübert and P. J. Hirschfeld, Phys. Rev. Lett. **80**, 4963 (1998).
[16] I. Vekhter, J. P. Carbotte, and E. J. Nicol, Phys. Rev. B **59**, 7123 (1999).
[17] I. Vekhter, P. J. Hirschfeld, J. P. Carbotte, and E. J. Nicol, Phys. Rev. B **59**, R9023 (1999).
[18] Yu. S. Barash, V. P. Mineev, and A. A. Svidzinskii, Pis'ma Zh. Eksp. Teor. Fiz. **65**, 606 (1997) [JETP Lett. **65**, 638 (1997)]; Yu. S. Barash and A. A. Svidzinskii, Phys. Rev. B **58**, 6476 (1998).
[19] G. E. Volovik (unpublished); K. A. Moler, A. Kapitulnik, D. J. Baar, R. Liang, and W. N. Hardy, Phys. Chem. Solids **56**, 1899 (1995).
[20] N. D. Whelan and J. P. Carbotte, cond-mat/0004152 (unpublished).
[21] Ch. Renner, B. Revaz, K. Kadowaki, I. Maggio-Aprile, and Ø. Fischer, Phys. Rev. Lett. **80**, 3606 (1998).
[22] S. H. Pan, E. W. Hudson, A. K. Gupta, K.-W. Ng, H. Eisaki, S. Uchida, and J. C. Davis, Phys. Rev. Lett. **85**, 1536 (2000).
[23] I. Maggio-Aprile, Ch. Renner, A. Erb, E. Walker, and Ø. Fischer, Phys. Rev. Lett. **75**, 2754 (1995).
[24] R. Cubitt *et al.*, Nature (London) **365**, 407 (1993).
[25] C. Caroli, P. G. de Gennes, and J. Matricon, Phys. Lett. **9**, 307 (1964).
[26] M. Franz and Z. Tešanović, Phys. Rev. Lett. **80**, 4763 (1998).
[27] K. Yasui and T. Kita, Phys. Rev. Lett. **83**, 4168 (1999).
[28] K. Maki and T. Tsuneto, Prog. Theor. Phys. **27**, 228 (1960).
[29] S. K. Yip and J. A. Sauls, Phys. Rev. Lett. **69**, 2264 (1992).
[30] M. Tinkham, *Introduction to Superconductivity* (McGraw-Hill, New York, 1996).
[31] C. P. Bidinosti, W. N. Hardy, D. A. Bonn, R. Liang, Phys. Rev. Lett. **83**, 3277 (1999); A. Carrington, R. W. Giannetta, J. T. Kim, and J. Giapintzakis, Phys. Rev. B **59**, R14 173 (1999).
[32] Y. Wang and A. H. MacDonald, Phys. Rev. B **52**, 3876 (1995).
[33] See, for example, H. Ding, M. R. Norman, T. Yokoya, T. Takeuchi, M. Randeria, J. C. Campuzano, T. Takahashi, T. Mochiku, and K. Kadowaki, Phys. Rev. Lett. **78**, 2628 (1997).
[34] J. Mesot, M. R. Norman, H. Ding, M. Randeria, J. C. Campuzano, A. Paramekanti, H. M. Fretwell, A. Kaminski, T. Takeuchi, T. Yokoya, T. Sato, T. Takahashi, T. Mochiku, and K. Kadowaki, Phys. Rev. Lett. **83**, 840 (1999).
[35] L. P. Gor'kov and J. R. Schrieffer, Phys. Rev. Lett. **80**, 3360 (1998).
[36] P. W. Anderson, cond-mat/9812063 (unpublished).
[37] A. S. Mel'nikov, J. Phys.: Condens. Matter **11**, 4219 (1999).
[38] M. Franz and Z. Tešanović, Phys. Rev. Lett. **84**, 554 (2000).
[39] L. Marinelli, B. I. Halperin, and S. H. Simon, Phys. Rev. B **62**, 3488 (2000).
[40] M. Chiao, R. W. Hill, C. Lupien, L. Taillefer, P. Lambert, R. Gagnon, and P. Fournier, Phys. Rev. B **62**, 3554 (2000).
[41] A. S. Mel'nikov, cond-mat/0007156 (unpublished).
[42] N. B. Kopnin and G. E. Volovik, Pis'ma Zh. Eksp. Teor. Fiz. **64**, 641 (1996) [JETP Lett. **64**, 690 (1996)].
[43] D. Knapp, C. Kallin, and A. J. Berlinsky, cond-mat/0011053 (unpublished).
[44] L. Marinelli (private communication).
[45] A. C. Durst and P. A. Lee, Phys. Rev. B **62**, 1270 (2000).
[46] P. J. Hirschfeld, D. Vollhardt, and P. Wölfle, Solid State Commun. **59**, 111 (1986); S. Schmitt-Rink, K. Miyake, and C. M. Varma, Phys. Rev. Lett. **57**, 2575 (1986).
[47] P. J. Hirschfeld and N. Goldenfeld, Phys. Rev. B **48**, 4219 (1993).
[48] J. H. Han and D. H. Lee, Phys. Rev. Lett. **85**, 1100 (2000).
[49] M. Franz and Z. Tešanović cond-mat/0002137(unpublished).
[50] M. Franz, Phys. Rev. Lett. **82**, 1760 (1999).
[51] I. Vekhter and P. J. Hirschfeld, Physica C **341-348**, 1947 (2000).
[52] I. Vekhter, L. N. Bulaevskii, A. E. Koshelev, and M. P. Maley, Phys. Rev. Lett. **84**, 1296 (2000).
[53] J. Ye, cond-mat/0003251 (unpublished).
[54] F. Yu, M. Salamon, A. J. Leggett, W. C. Lee, and D. M. Ginzberg, Phys. Rev. Lett. **74**, 5136 (1995).
[55] R. Wortis, A. J. Berlinsky, and C. Kallin, Phys. Rev. B **61**, 12 342 (2000).
[56] S. H. Simon and P. A. Lee, Phys. Rev. Lett. **78**, 1548 (1997); **78**, 5029 (1997); G. E. Volovik and N. B. Kopnin, *ibid.* **78**, 5028 (1997).
[57] H. Won and K. Maki, Phys. Rev. B **53**, 5927 (1996).
[58] I. S. Gradshteyn and I. M. Ryzhik, *Table of Integrals, Series, and Products* (Academic Press, London, 1980).
[59] V. G. Kogan, Phys. Rev. B **24**, 1572 (1981).
[60] E. Schachinger and J. P. Carbotte, Phys. Rev. B **60**, 12 400 (1999).
[61] H. Won and K. Maki, cond-mat/0004105 (unpublished).
[62] I. Vekhter, P. J. Hirschfeld, J. P. Carbotte, and E. J. Nicol, in *Physical Phenomena at High Magnetic Fields-III*, edited by Z. Fisk, L. Gor'kov, and R. Schrieffer (World Scientific, Singapore, 1999), pp. 410–413; also available as cond-mat/9811315.
[63] H. Won, H. Jang, and K. Maki, cond-mat/9901252 (unpublished).
[64] K. Yang and S. Sondhi, Phys. Rev. B **57**, 8566 (1998); J. Appl. Phys. **87**, 5549 (2000).
[65] L. Taillefer, B. Lussier, R. Gagnon, K. Behnia, and H. Aubin, Phys. Rev. Lett. **79**, 483 (1997).
[66] D. K. Morr and R. Wortis, Phys. Rev. B **61**, R882 (2000).
[67] I. Vekhter, J. P. Carbotte, P. J. Hirschfeld, and E. J. Nicol, in *High-Temperature Superconductivity*, edited by S. E. Barnes *et al.* (AIP, Melville, NY, 1999), pp. 341–346.
[68] G.-q. Zheng, Y. Kitaoka, K. Asayama, and Y. Kodama, Physica C **227**, 169 (1994).